An improved perspective in the spatial representation of soil moisture: potential added value of SMOS disaggregated 1 km resolution "all weather" product

Samiro Khodayar[1], Amparo Coll[2], Ernesto Lopez-Baeza[2]

[1] Institute of Meteorology and Climate Research (IMK-TRO), Karlsruhe Institute of

Technology (KIT), Karlsruhe, Germany

[2] University of Valencia, Spain. Earth Physics and Thermodynamics Department. Climatology

from Satellites Group

Submitted to HESS

* Corresponding author. E-mail address: samiro.khodayar@kit.edu (S. Khodayar)

Institute for Meteorology and Climate Research, Karlsruhe Institute of Technology (KIT),

Postfach 3640, 76021 Karlsruhe, Germany

1   **Abstract**

2   This study uses the synergy of multiresolution soil moisture (SM) satellite estimates from the

3   Soil Moisture Ocean Salinity (SMOS) mission, a dense network of ground-based SM

4   measurements, and a Soil Vegetation Atmosphere Transfer (SVAT) model, SURFEX

5   (Externalized Surface) – module ISBA (Interactions between Soil-Biosphere-Atmosphere), to

6   examine the benefits of the SMOS L4 version 3.0 or "all weather" high resolution soil

7   moisture disaggregated product (~ 1 km, SMOS_L4$^{3.0}$). The added value compared to

8   SMOS-L3 (~ 25 km) and L2 (~15 km) is investigated. In situ SM observations over the

9   Valencia Anchor Station (VAS; SMOS Calibration/Validation (Cal/Val) site in Europe) are

10   used for comparison. The SURFEX(ISBA) model is used to simulate point-scale surface SM

11   (SSM) and, in combination with high-quality atmospheric information data, namely ECMWF

12   and the SAFRAN meteorological analysis system, to obtain a representative SSM mapping

13   over the VAS. The sensitivity to realistic initialization with SMOS_L4$^{3.0}$ to simulate the

14   spatial and temporal distribution of SSM is assessed. Results demonstrate: (a) all SMOS

15   products correctly capture the temporal patterns, but, the spatial patterns are not accurately

16   reproduced by the coarser resolutions probably in relation to the contrast with point-scale in

17   situ measurements. (b) The potential of SMOS-L4$^{3.0}$ product is pointed out to adequately

18   characterize SM spatio-temporal variability reflecting patterns consistent with intensive point

19   scale SSM samples on a daily time scale. The restricted temporal availability of this product

20   dictated by the revisit period of the SMOS satellite compromises the averaged SSM

21   representation for longer periods than a day. (c) A seasonal analysis points out improved

22   consistency during December-January-February and September-October-November in

23   contrast to significantly worse correlations in March-April-May (in relation to the growing

24   vegetation) and June-July-August (in relation to low SSM values < 0.1 m^3/m^3 and low spatial

25   variability). (d) The combined use of the SURFEX(ISBA) SVAT model with the SAFRAN

26 system, initialized with SMOS-L4$^{3.0}$ 1 km disaggregated data is proven to be a suitable tool to

27 produce regional SM maps with high accuracy which could be used as initial conditions for

28 model simulations, flood forecasting, crop monitoring and crop development strategies,

29 among others.

30 *Key Words: soil moisture, SMOS 1-km disaggregated product, SURFEX, Valencia Anchor*

31 *Station, realistic initialization, SAFRAN*

32

33

34

35

36

37

38

39

40

41

42

43

44

45

1. Introduction

Reliability of climate and hydrological models is constrained by associated uncertainties, such as input parameters. Among them, soil moisture is a variable of pivotal importance controlling the exchanges of water and energy at the surface/atmosphere interface (Entekhabi et al., 1996). Thus, it is a highly relevant variable for climate, hydrology, meteorology and related disciplines (e.g. Seneviratne et al. 2010).

Soil moisture is greatly variable spatially, temporally and across scales. The spatial heterogeneity of soil, vegetation, topography, land cover, rainfall and evapotranspiration are accounted responsible (Western et al., 2002; Bosh et al., 2007; Rosenbum et al. 2012).

The response of soil moisture to precipitation changes largely depends on soils water capacity and climatic zones. Particularly, in dry climates such as the Iberian Peninsula (IP), soil moisture quickly reacts to changes in precipitation (Li and Rodell 2013). Precipitation variability and mean are positively correlated, thus, an increase in precipitation yields wetter soils, which in turn results in higher spatial variability of soil moisture. An adequate representation of the high spatio-temporal variability of soil moisture is needed to improve climate and hydrological modelling (Koster et al., 2004; Seneviratne et al., 2006; Brocca et al., 2010). Its impact has been seen on time scales from hours to years (e.g., ~ 20 km scale: Taylor and Lebel, 1998; droughts: Schubert et al., 2004; decadal drying of the Sahel: Walker and Rowntree, 1977; hot extremes: Seneviratne et al., 2006b; Hirschi et al., 2011; decadal simulations: Khodayar et al., 2014). To obtain an appropriate representation of this variable, especially at high-resolution, is not an easy task mainly because of its high variability. Methods for the estimation of soil moisture can be divided in three main categories, (i) measurement of soil moisture in the field, (ii) estimation via simulation models, and (iii) measurement using remote sensing. In general, in situ measurements are far from global (e.g., Robock et al. 2000), and model simulations present important biases. Therefore, we have to

71 rely on space-borne sensors to provide such measurements, but until recent times no

72 dedicated, long-term, moisture space mission was attempted (Kerr, 2007).

73 Nowadays, by means of remote sensing technology surface soil moisture is available at global

74 scale (Wigneron et al., 2003). The best estimations result from microwave remote sensing at

75 low frequencies (e.g. Kerr, 2007; Jones et al., 2011) and several global soil moisture products

76 have been produced, such as the European Space Agency's Climate Change Initiative (ESA

77 CCI, Liu et al. 2011; Wagner et al. 2012) soil moisture products, the soil Moisture Active

78 Passive (SMAP; Entekhabi et al. 2010), the Advanced Microwave Scanning Radiometer-EOS

79 (AMSR-E; Owe et al. 2008), the advanced scatterometer (ASCAT; Naeimi et al. 2009) and

80 the Soil Moisture and Ocean Salinity (SMOS; Kerr et al., 2001) .

81 The SMOS mission is the first space-borne passive L-band microwave (1.4 GHz) radiometer

82 measuring at low frequency soil moisture over continental surfaces as well as ocean salinity

83 (Kerr et al., 2001, 2010). SMOS delivers global surface soil moisture measurements (~ 0-5

84 cm depth) at 0600 a.m. and 0600 p.m. LT (local time) in less than 3-days revisit at a spatial

85 resolution of ~ 44 km. The benchmark of the mission is to reach accuracy better than 0.04

86 m^3/m^3 for the provided global maps of soil moisture (Kerr et al., 2001).

87 SMOS data is not exempt of biases. Validating remote sensing-derived soil moisture products

88 is difficult, e.g. due to scale differences between the satellite footprints and the point

89 measurements on the ground (Cosh et al., 2004). However, in the last years a huge effort has

90 been made to validate the SMOS algorithm and its associated products. With this purpose, in

91 situ measurements across a range of climate regions were used assessing the reliability and

92 accuracy of these products using independent measurements (Delwart et al., 2008; Juglea et

93 al., 2010; Bircher et al., 2012; Dente et al., 2012; Gherboudj et al., 2012; Sánchez et al., 2012;

94 Wigneron et al., 2012). The strategy adapted by the European Space Agency (ESA) was to

95 develop specific land product validation activities over well-equipped monitoring sites. An

96   example for this is the Valencia Anchor Station (VAS; Lopez-Baeza et al., 2005a) in eastern

97   Spain, which was chosen as one of the two main test sites in Europe for the SMOS

98   Calibration/Validation (Cal/Val) activities. The validation sites were chosen to be slightly

99   larger than the actual pixel (3dB footprint), thus, VAS covers a 50x50 km^2 area. Within this

100 area, a limited number of ground stations were installed relying on spatialized soil moisture

101 information using the SVAT (Soil Vegetation Atmospheric Transfer) SURFEX (Externalized

102 Surface) model. Worldwide validation results reveal a coefficient of determination (R^2) of

103 about 0.49 when comparing the ~5 cm in situ soil moisture averages and the SMOS soil

104 moisture level 2 (SMOS-L2 ~ 15 km). For example, validation results by Bircher et al. (2012)

105 in Western Denmark show R^2 of 0.49-0.67 (SMOS retrieved initial soil moisture) and 0.97

106 (SMOS retrieved initial temperature). Besides, a significant under-/over-representation of the

107 network data (biases of − 0.092-0.057 m^3/m^3) is also found. Over the Maqu (China) and the

108 Twente (The Netherlands) regions, the validation analysis resulted in R^2 of 0.55 and 0.51,

109 respectively, for the ascending pass observations, and of 0.24 and 0.41, for the descending

110 pass observations. Furthermore, Dente et al. (2012) pointed out a systematic SMOS soil

111 moisture (ascending pass observations) dry bias of about 0.13 m^3/m^3 for the Maqu region and

112 0.17 m^3/m^3 for the Twente region. Validation of the SMOS level 3 product (SMOS-L3 ~ 35

113 km) shows that the general dry bias in SMOS-L2 is also present in SMOS-L3 SM. This bias

114 is markedly present in the ascending products and shorter time series as described in Sanchez

115 et al. (2012) and Gonzalez-Zamora et al. (2015). In this case, the presence of dense vegetation

116 is seen to increase RMSE scores, whereas in low vegetated areas a lower dry bias is found

117 (Louvet et al. 2015).

118 Since the launch of the SMOS satellite, the processing prototypes of the SMOS L2 soil

119 moisture have evolved, and their quality has improved. Furthermore, efforts have been made

120 to cover the need of a reliable product with finer resolution for hydrological and climatic

121 studies where the spatial variability of soil moisture plays a crucial role, e.g. in the estimation

122 of land surface fluxes (evapotranspiration (ET) and runoff). Piles et al. (2011) presented a

123 downscaling approach to optimally combine SMOS´ soil moisture estimates with MODIS

124 (Moderate Resolution Imaging Spectroradiometer) visible/infrared (VIS/IR) satellite data into

125 1 km soil moisture maps over the IP without significant degradation of the root mean square

126 error (RMSE). This product has been evaluated using the REMEDHUS (REd de MEDicion

127 de la HUmedad del Suelo) soil moisture network in the semi-arid area of the Duero basin,

128 Zamora, Spain (Piles et al. 2014). Results show that downscaling maintains temporal

129 correlation and root mean squared differences with ground-based measurements, hence,

130 capturing the soil moisture dynamics. Complementary studies after Piles et al. (2011) have

131 produced similar downscaled high-resolution SMOS-L4 soil moisture products (e.g.

132 Malbéteau et al (2018); Djamai et al (2016)). Being similar, however, the algorithms

133 originating them are totally different from those of SMOS-L4 used in this study. Whereas

134 SMOS-L4 products in this study proceed from the original SMOS-L2 (15 km resolution soil

135 moisture) disaggregated by 1-km MODIS LST and NDVI, Malbéteauet al (2018) and

136 Djamaiet al (2016) products proceed from the original SMOS-L1 (15 km resolution

137 brightness temperature).

138 A big limitation for the downscaling approach used in Piles et al. (2011) is the lack of

139 information in cloudy conditions of the hereafter named SMOS_L4$^{2.0}$, which significantly

140 limits the availability and usefulness of this product. In this study, we examine a new version

141 of the SMOS_L4 product, the SMOS Level 4 3.0 "all weather" disaggregated ~ 1 km SM

142 (SMOS_L4$^{3.0}$), which was developed and has been recently made available by SMOS-BEC

143 (Barcelona Expertise Centre).In this advanced high-resolution soil moisture product the

144 limitation on clouds is modulated by the use of ERA-Interim LST data, thus providing soil

145 moisture measurements independently of the cloud conditions.

146 Contrary toSMOS-L3 and -L2 products, which have been extensively validated as described

147 above and used for assimilation purposes in models (e.g. De Lannoy et al. 2016; Leroux et al.

148 2016), few studies deal with the disaggregated 1 km SMOS-L4$^{0.2}$ and SMOS-L4$^{0.3}$ products

149 (mostly in relation to wildfire activity) and validation efforts have concentrated only on the

150 REMEDHUS soil moisture network in Zamora (north-western Spain; e.g. Piles et al. 2014).

151 The objective of this paper is to provide information about the advantages and drawbacks and

152 the added value of the disaggregated 1 km SMOS-L4$^{3.0}$ "all weather" soil moisture product

153 with respect to coarser resolution products. The proposed investigation covers a one year

154 period (a complete hydrological cycle) and focuses on the semi-arid VAS area (eastern Spain)

155 and the IP where water availability and fire risk are big environmental issues, thus, knowledge

156 of soil moisture conditions is of pivotal importance. Furthermore, as spring time soil moisture

157 anomalies over the IP are believed to be a pre-cursor to droughts and heat waves in Europa

158 (Vautard et al. 2007; Zampieri et al. 2009), accurate monitoring and prediction of surface

159 states in this region may be key for improvements in seasonal forecasting systems.

160 The following objectives are then pursued: (a) Examination of soil moisture temporal and

161 spatial distribution with SMOS-derived soil moisture products over the investigation domain

162 using a multi-resolution approach: L3 (~ 25 km), L2 (~15 km), and L4$^{3.0}$ (~ 1 km), (b)

163 Validation with the in situ soil moisture measurements' network (VAS) to estimate the

164 reliability of the SMOS SM products, and (c) Evaluation of the impact of realistic SM

165 initialization using SMOS-L4$^{3.0}$ on point-scale and regional SURFEX(ISBA) model

166 simulations over the VAS area.

167 This investigation is structured as follows, in Section 2, the study area and the data sets are

168 presented including the in situ network measurements, the SMOS data products, and the

169 SURFEX(ISBA) model and related atmospheric forcings used. Section 3 summarizes the

170 methodology applied. The results are discussed in Section 4. Finally, conclusions are drawn in

171 Section 5.

172

173 **2. Study area and data set**

174 2.1 Investigation domain and in situ measurements over the VAS

175 The main investigation areas in this study are the Iberian Peninsula and the Valencia Anchor

176 Station (VAS) site located in eastern Spain (39.69°-39.22° N,-1.7°-(-1.11°) W). The VAS site

177 covering approximately a 50x50 km^2 area was established in December 2001 by the

178 University of Valencia as a Calibration/Validation (Cal/Val) site for different low-resolution

179 Earth Observation data products (Bolle et al., 2006). The extension and homogeneity of the

180 area as well as the mostly flat conditions (slopes lower than 2%) make it an ideal reference

181 site. Nevertheless, the small variations in the area, 750 to 950 m, influence the climate of the

182 region, which oscillates between semiarid to dry-sub-humid. Most of the area is dedicated to

183 vineyards (65%), followed by trees, shrubs, forest and industrial and urban cover types.

184 Mostly bare soil conditions are observed beside the vineyard growing season (March/April to

185 September/October). Mean temperatures in the region are between 12°C and 14°C with

186 annual mean precipitation about 450 mm, with maximums in spring and autumn. Within the

187 VAS, a network consisting of eight ThetaProbe ML2x soil moisture stations was deployed by

188 the Climatology from Satellites Group from the Earth Physics and Thermodynamics

189 Department at the University of Valencia. The eight in situ stations are distributed over a

190 10x10 km^2 area (Figure 1), according to land use, soil type, and other environmental

191 conditions. Details about the characteristics of each station are summarized in Table 1. Soil

192 moisture measurements every 10 min, mostly from 2006, were carried out for the top first 5

193 cm. More details about the VAS characteristics and soil moisture measurements could be

194 found in Juglea et al. (2010). Precipitation measurements over the IP and the VAS are from

195 the AEMET (Agencia Estatal de Meteorología; Spanish Weather Service) network.

196 Measurements every 10 min are available.

197 2.2 The SMOS surface soil moisture products

198 ESA's derived SMOS Soil Moisture Level 2 (SMOS-L2) data product, ~ 15 km, contains the

199 retrieved soil moisture and optical thickness and complementary parameters such as

200 atmospheric water vapour content, radio frequency interferences and other flags. The SMOS-

201 L2 algorithms have been refined since the launch of SMOS, resulting in more precise SM

202 retrievals (ARRAY, 2014). The Level 3 SM product, SMOS-L3, was obtained from the

203 operational CATDS archive. This is a daily product that contains filtered data. The best

204 estimation of SM is selected for each node when several multi-orbit retrievals are available

205 for a given day. A detection of particular events is also performed in order to flag the data.

206 The processing of the data separates morning and afternoon orbits. The aggregated products

207 are generated from this fundamental product. The Level 4 SM, SMOS-L4 2.0 data (SMOS-

208 L4$^{2.0}$), with 1 km spatial resolution is provided by BEC and covers the IP, Balearic Islands,

209 Portugal, South of France, and North of Morocco (latitudes 34°− 45° N and longitudes 10° W

210 − 5° E). A downscaling method that combines highly accurate, but low-resolution SMOS

211 radiometric information (SMOS-L2 data) with high-resolution (brightness temperature

212 measurements), but low sensitivity, visible-to-infrared imagery (NDVI (Normalized

213 Difference vegetation Index) and LST (Land Surface Temperature) from Aqua MODIS) to

214 SSM across spatial scales is used to derive the SMOS-L4$^{2.0}$ data (Piles et al 2010). The impact

215 of using different vegetation indices from MODIS with higher spatial and temporal resolution

216 in the downscaling method was explored in Sanchez-Ruiz et al. (2014), showing that the use

217 of more frequent and higher spatial-resolution vegetation information lead to improved SM

218 estimates. The latest SMOS-L4 product is the version 3.0 or "all weather" (SMOS-L4$^{3.0}$),

which is the product used and examined in this study. The downscaling approach is based on Piles et al. (2014) and Sanchez-Ruiz et al. (2014), with the novelty of introducing ERA-Interim LST data in the MODIS LST/NDVI scape, thus providing soil moisture measurements independently of the cloud conditions. ERA-Interim provides a resolution of about 0.125°, whereas MODIS is a ~ 1 km product. The evaluation of the SMOS-L4 2.0 and 3.0 products support the use of the "all weather" version, since it does not depend on cloud cover and the accuracy of the estimates with respect to in-situ data is improved or preserved (Piles et al. (2015), SMOS-BEC Team (2016)).

In this study, the SMOS-L2 V5.51 data coming from a L1C input product (obtained from MIRAS measurements), the SMOS-L3 V2.72 and the SMOS-L4 V3.0 are employed.

2.3 The SURFEX(ISBA) SVAT model

The SVAT model SURFEX (Externalized Surface, Le Moigne et al. 2009) − module ISBA (Interactions between Soil-Biosphere-Atmosphere, Noilhan and Planton 1989) is used to generate point-scale and spatially distributed SM spatial at 1 km grid spacing and temporal fields from initial conditions and atmospheric forcing. SURFEX(ISBA) was developed at the National Center for Metorological Research (CNRM), at Météo France, and it has been widely validated over vegetated and bare surfaces (e.g. Calvet et al. 1998). The ISBA scheme uses the Clapp and Hornberger (1978) soil water model and Darcy's law for the estimation of the diffusion of water in the soil, and allows 12 land use and related vegetation parameterization types. Crops are considered for the VAS area since mainly vineyards, almond and olive trees and shrubs compose the region.

The surface characteristics are considered in the SVAT input, roughness and the fraction of vegetation are adopted from ECOCLIMAP (Masson et al. 2003), topography is obtained from GTOPO (GTOPO30 Documentation) and soil types are defined using FAO (FAO, 2014).

243 To obtain an accurate simulation of soil moisture in the study area, the model was originally

244 calibrated by Juglea et al. (2010) to be applied over the entire site for any season/year.

245 Particularly relevant for this study is the specific definition of the soil hydraulic parameters

246 which they made for the VAS area, since most of the hydrological parameters are site

247 dependent and not available from SMOS observations. A new set of empirical equations as a

248 function of the percentages of sand and clay was defined using Cosby et al. (1984) and Boone

249 et al. (1999). New definitions and recommendations by Juglea et al. (2010) for the VAS area

250 were adopted in this investigation.

251 *Atmospheric forcing information: ECMWF and SAFRAN*

252 High quality atmospheric forcing is needed to carry out accurate simulations. To run the

253 SURFEX(ISBA) model, the following atmospheric forcing data are needed: air temperature

254 and humidity at screen level, atmospheric pressure, precipitation, wind speed and direction

255 and solar and atmospheric radiation. Three different sets of atmospheric forcing information

256 are used in this study as input forcing for the SURFEX(ISBA) simulations; (a) SURFEX-

257 OBS: meteorological data from 3 fully equipped stations in the OBS area, MELBEX-I,

258 MELBEX-II and VAS, (b) SURFEX-ECMWF: ECMWF (European Centre for Medium-

259 Range Weather Forecast) data, and (c) SURFEX-SAFRAN: information from the SAFRAN

260 (Système d'Analyse Fournissant des Renseignements Atmosphériques à la Neige)

261 meteorological analysis system (Durand et al. 1999; Quintana-Seguí et al. 2008; Vidal et al.

262 2010).

263 Precipitation, air temperature, surface pressure, air specific humidity, wind speed and

264 direction, downward longwave radiation, diffuse shortwave radiation, downward direct

265 shortwave radiation, snowfall rate and CO_2 concentration are used as input data from the

266 meteorological stations aforementioned in the OBS area. A temporal resolution of 10 min is

267 available. From ECMWF, dew point and temperature at 2 m, pressure, precipitation and wind

268 components, are used as forcing data, with a 6 h temporal resolution and 0.125°x0.125°

269 spatial resolution. Precipitation, air temperature, surface pressure, air specific humidity, wind

270 speed and downward shortwave and longwave radiation from SAFRAN are used as input

271 information with a spatial resolution of 8x8 km^2 and an hourly temporal resolution. In this last

272 case, we have an optimal spatial and temporal distribution of the atmospheric forcing over the

273 VAS area (~ 50x50 km^2) and a rare to find complete database to force the land surface model.

274 More details about the SAFRAN system and its validation in north-eastern Spain could be

275 found in Quintana-Seguí et al. (2016).

276

277 **3. Analysis methodology**

278 In order to investigate the characteristics and potential added values of fine-scale SMOS-

279 derived soil moisture, the spatial variability, the temporal evolution as well as the probability

280 distribution is investigated. With this purpose, SMOS-derived soil moisture products at

281 different spatial resolutions, in situ measurements and model simulations are jointly

282 evaluated.

283 The spatial distribution and temporal evolution of precipitation and SMOS-derived soil

284 moisture over the IP and the VAS area are assessed for the time period from December 2011

285 to December 2012 considering also hydrological seasons (DJF: December-January-February,

286 MAM: March-April-May, JJA: June-July-August, SON: September-October-November).

287 Special attention is paid to the autumn season since in this period the western Mediterranean

288 is characterized by a large thermal gradient between the atmosphere and the sea (Duffourg

289 and Ducrocq, 2011, 2013) resulting in intense precipitation extremes (Raveh-Rubin and

290 Wernli 2015). Furthermore, during 2012, the Hydrological Cycle in the Mediterranean

291 Experiment (HyMeX; Dobrinski et al. 2014) took place in the Western Mediterranean with

292   the IP and particularly the Valencia region as target areas. During the SON period of 2012,

293   the Special Observation Period (SOP1; Ducrocq et al. 2014) with intensive experimental

294   deployment over the area took place. This provides us with valuable information about the

295   environmental conditions as well as the occurrence of precipitation events in the investigation

296   area. Particularly, precipitation in the IP during the autumn (SON) period of 2012 was above

297   average (Khodayar et al. 2015). It was also the hydrological season in which higher variability

298   in the soil moisture was observed as a result of the precipitation distribution. Two unique

299   events, at the end of September (27-29) affecting south and eastern Spain and at the end of

300   November (19-20) affecting the Ebro valley (Jansà et al. 2014), largely determined the

301   positive anomaly in precipitation and soil moisture in this period.

302   SMOS-L3 (~ 25 km), SMOS-L2 (~ 15 km), and SMOS-L4$^{3.0}$ (~ 1km) are used for the

303   evaluation of soil moisture distribution at different grid spacing. Piles et al. (2014) pointed out

304   that differences may exist between SMOS-L3–L2 and the 1 km disaggregated soil moisture

305   SMOS-L4 because of the distinct methodology used to obtain these products. Only SMOS

306   descending passes or a mean between ascendant and descent passes are used to calculate

307   mean daily values of SMOS-derived soil moisture. Soil moisture derived from the afternoon

308   orbits was found to be more accurate than the morning passes (Piles et al. 2014). The fine

309   temporal resolution of the model simulations (1 h) and the observations (10 min) allow

310   comparisons at the time of the SMOS overpasses. Because of the 3-day revisit period of the

311   SMOS swath, the IP will not be fully covered by the satellite on daily basis. However, despite

312   identified difficulties (radio frequency interferences, missing data ...), the IP is well observed

313   being 1.5 days the average observations frequency over the IP. Only those images with

314   coverage higher than 50% are considered in our calculations. A conservative remapping to

315   coarser resolutions is applied, when required, to make comparisons among each other or with

316   respect to ground-based observations on equal terms. Remapping allows point to point

317 comparisons between these data sets. In addition to the yearly and seasonal approach, an

318 exemplary short time period, 19 to 20 October of 2012, is considered. This corresponds to one

319 of the periods in which an extreme precipitation event occurred in the Ebro valley (at the end

320 of November; Jansà et al. 2014. Therefore, high variability in the soil moisture distribution is

321 expected.

322 The coefficient of variation (CV), defined as the ratio of the standard deviation to the mean,

323 of the precipitation and soil moisture fields over the IP, the VAS (50x50 km2) and the OBS

324 (10x10 km2) area are examined for the analysis of the spatial variability and its evolution in

325 time. The soil moisture daily index ($SM_{index,i}$) is calculated to assess the evolution pattern

326 allowing the study of daily variations

327 $SM_{index,i} = (SM_{i+1} - SM_i)/ SM_i$, where SM_{i+1} is the soil moisture of the day i+1 and SM_i is the

328 soil moisture of the day before i.

329 For these calculations, SMOS afternoon (descendant; Piles et al. 2014) orbits are selected as

330 well as observations at the time of the SMOS overpasses. For the IP and VAS, SMOS-L2 and

331 SMOS–L4$^{3.0}$ have been remapped to the coarser grid spacing for an adequate comparison.

332 Ground-based observations are aggregated using a mean over all stations for comparison with

333 the corresponding SMOS-L4$^{3.0}$ data (the closest grid point is selected).

334 The reliability of SMOS-L3, SMOS-L2 and SMOS-L4$^{3.0}$ soil moisture products is evaluated

335 by comparison with in situ soil moisture measurements in the OBS area. The spatial and

336 temporal variability are considered as well as the probability distribution. Different

337 approaches are applied: (a) the nearest grid point is selected for point-like comparisons

338 between SMOS-L2 and SMOS-L4$^{3.0}$ against in situ soil moisture stations, to reduce sampling

339 biases in this region of diverse soil characteristics (Table 1), (b) SMOS-L4$^{3.0}$ soil moisture

340 grid cells are averaged over the 10x10 km^2 area and compared to the mean from the soil

341   moisture network stations to address the issue related to spatial averaging due to the high

342   spatial and temporal variability of the upper-most SSM. For the comparison between the

343   SMOS-L2 and the in situ observations: when single ground-based stations are considered the

344   closest SMOS pixel is selected, in case of considering the OBS (10x10 km^2) or VAS (50x50

345   km^2) areas the mean over all pixels which centre falls within the area is used. For the

346   comparison with SMOS descending passes the corresponding values from in situ

347   measurements are considered. Additionally, a separation between wet days (precipitation over

348   1 mm/d) and dry days is applied to consider possible implications of wet/dry soils for SMOS

349   measurements.

350   Linear regression, the coefficient of determination (R^2), the mean bias (MB), and the root

351   mean square deviation (RMSD) are used to predefine the accuracy. A debiased or centred

352   RMSD (CRMSD) is applied to discriminate the systematic and random error components

353   removing the overall bias before calculating the RMSD.

354   Soil moisture modeling is performed by the use of the SVAT, SURFEX (Externalized

355   Surface) – module ISBA (Interactions between Soil-Biosphere-Atmosphere) from Météo-

356   France. Configuration and specifications described in Juglea et al. (2010), which proved

357   successful in adequately simulate the associated soil moisture heterogeneity over the wide

358   VAS surface (50x50 km^2), are adapted in this study. Simulations start on 1 December 2011 at

359   00UTC and cover the whole investigation period until 31 December 2012 with an hourly-

360   output time resolution. Point-scale SURFEX(ISBA) simulations over the soil moisture

361   network stations in the VAS domain are validated with the in situ measurements to assess the

362   usefulness of the model for further investigation, picturing the potential of the model in

363   simulating upper level soil moisture variability on different soil characteristics (Table 1).

364   To try to simulate the spatial and temporal heterogeneity of the soil moisture fields over the

365   VAS surface, the SURFEX(ISBA) scheme is used in combination with high quality forcing

data from ECMWF (hereafter SURFEX-ECMWF) and the SAFRAN system (hereafter SURFEX-SAFRAN) for spatialization purposes. Soil moisture initialization in spatialized SURFEX(ISBA) simulations requires a single representative value for the whole simulation area. The benefit of initializing the simulations with SMOS-L4$^{3.0}$ data in comparison to climatological means is discussed. In-situ soil moisture observations over the VAS area are considered for verification. A comparison between SURFEX-SAFRAN point-scale and 10x10 km^2 mean simulations initialized with SMOS-L4$^{3.0}$ data is done against ground measurements to assess the accuracy of the simulated SSM maps.

4. Results

4.1 SMOS-derived soil moisture at different resolutions

4.1.1 Spatial variability on seasonal and sub-seasonal time scales

Figure 2a shows the north-south precipitation gradient for the SON period mean. The SSM satisfactorily reflects this gradient (Figure 2b), but, more markedly for the SMOS-L3 and SMOS-L2 than the higher resolution SMOS-L4$^{3.0}$ showing lower standard deviation, SMOS-L3(~0.15±0.01), SMOS-L2(~0.17±0.01), SMOS-L4(~0.22±0.007). The same performance is seen over the VAS domain (not shown). The SSM variability associated to the extreme precipitation events in this period is not well represented in the SMOS-L4$^{3.0}$ seasonal mean. Table 2 shows the number of days (percentage) in which there is more than 50 % of data over the IP for each SMOS product. These periods have been used as basis for the calculation of the spatial distributions in Figure 2b. SMOS-L3 (88 %) and SMOS-L2 (84 %) show a good coverage and similar number of days. However, a large difference is observed with respect to the SMOS-L4$^{2.0}$ product with only 28 days (32 %) of adequate coverage for the period of SON 2012. This is due to the problematic associated to the downscaling approach used to

390   obtain the 1 km soil moisture maps, in which the lack of Land Surface Temperature (LST)

391   information from MODIS visible/infrared (VIS/IR) satellite data in cloudy conditions (section

392   2.2) constrains derived-SSM information. The availability and usefulness of this product is

393   therefore significantly reduced. The new product L4$^{3.0}$, used in this study, in which the

394   previous limitation is resolved using ERA-Interim-derived LST information, shows a

395   coverage percentage in the order of 92 %, even higher than the SMOS-L3 and -L2 products.

396   However, Figure 2b demonstrates that the spatial representation of the seasonal mean does not

397   improve with this product, as a consequence of the limited temporal availability of the

398   SMOS-derived SSM product dictated by the revisit period of the satellite.

399   In Figure 3, only common available days from all different operational levels are selected for

400   an inter-SMOS product comparison. When remapped to the same resolution (coarser grid

401   spacing) comparable values are identified between SMOS-L3, -L2 and –L4$^{3.0}$ for the JJA and

402   SON period, whereas relevant differences are pointed out from December to May. In this last

403   period, we identify higher means for the SMOS-L4$^{3.0}$ product and SMOS-L3 with respect to

404   SMOS-L2, which is in agreement with a systematic dry bias identified for SMOS-L2 also in

405   previous studies (section 1).

406   At sub-seasonal scales, e.g. event scale on the 19-20 November 2012 (Figure 4), the SMOS-

407   L4$^{\mathbf{3.0}}$ product shows SSM mean and variability in the same range of the SMOS-L2 and -L3

408   products, but with a finer-improved resolution representation of the spatial distribution.

409   Comparisons with the mean ground-based SSM at the VAS (OBS area: *0.25 ±0.0002*) show

410   better agreement with the mean SSM from the SMOS-L4$^{3.0}$-1 km disaggregated product

411   (*0.23±0.002*) and poorer correlation with SMOS-L2 (*0.20±0.002*). The problematic of SMOS-

412   L4$^{3.0}$ on seasonal time scales vanishes at sub-seasonal (event) scales where the potential

413   added value of the 1 km product is manifest.

414   4.1.2 Temporal evolution of surface soil moisture data sets

415   The SMOS and in situ measured SSM time series are investigated and compared in this

416   section in Figures 5 and 6 over the IP, the VAS (50x50 km2) and the OBS (10x10 km2) areas.

417   Overall, the averaged SMOS-L2 and -L4$^{3.0}$ data over the IP are much more variable than the

418   SMOS-L3, showing a more extreme daily index (SMOS-L2: -1 to 2; SMOS-L4$^{3.0}$: -0.7 to

419   1.45). Over the VAS, SMOS-L2 is clearly more variable than the higher resolution SMOS-

420   L4$^{3.0}$. But, the last one shows a wider range of values as well as more extreme daily index

421   values when compared to the averaged in situ soil moisture measurements. The CVs of the

422   spatially averaged SMOS-L4$^{3.0}$ is lower than those of SMOS-L3, -L2 and in situ observations

423   indicating that this data are less scattered. Despite detected differences within in situ

424   observations, SMOS responds well to soil moisture variations over time.

425   Although absolute values are not totally captured, all three SMOS products adequately

426   reproduce the temporal dynamics at a regional scale. The systematic dry bias present on

427   SMOS-L2 data (Piles et al. 2014) is evident particularly on the first half of the year. A mean

428   bias in the order of -0.09 to -0.07 m^3/m^3 is identified for the DJF-MAM period; this difference

429   is reduced to -0.02 m^3/m^3 for the JJA-SON period (Table 3). During the DJF-MAM period the

430   vineyards are bare, only the vine stocks are present. The water content of the vine stocks

431   negatively impacts the SMOS measurements (Schwank et al. 2012).

432   Good agreement is found between the SMOS-L4$^{3.0}$ product and the mean of the in situ

433   observations (the network's variability (shaded grey) contains the SMOS-L4$^{3.0}$ data). Scores

434   confirm this result particularly for the periods DJF and SON (slope~1, R^2~0.7). Poorer

435   correlation is found for the MAM (slope~0.6, R^2~0.4). In this period, soil moisture maxima

436   immediately after the precipitation events are not always well captured by the SMOS-L4$^{3.0}$

437   data, showing additionally a too rapid drying after this. This observation agrees with the

438   SMOS' inability of correctly measuring in situations when liquid water is present at the soil.

439   The measured signal is perturbed during the vegetation growing season, which could explain

440 the worse statistics. On the other hand, during JJA, low slope~0.1 and R^2~0.01 could be in

441 relation to SSM values close to or lower than 0.1 m^3/m^3 and very low spatial variability,

442 which was found to be necessary for an adequate performance of the algorithm used for the

443 derivation of the SMOS-L4 1 km product in Molero et al. (2016).

444 4.2 Spatial comparison at high-resolution: SMOS-L4$^{3.0}$ versus ground measurements

445 High-resolution spatio-temporal correlations are assessed by spatial comparison with in situ

446 observations. Characteristics of each of the in-situ stations are presented in Table 1. A

447 seasonal analysis is performed focusing on the selected year of measurements covering a

448 complete hydrological cycle (from 1 December 2011 to 31 December 2012). Comparisons

449 between SMOS-L2 and ground measurements are additionally included. Statistics for

450 individual comparisons at all stations are summarized in Table 3. Comparisons between

451 SMOS-L3 and ground measurements were similarly performed evidencing the expected bad

452 correlations (R^2 ~ 0,002, not shown)In Figure 7, the scatter plots display (a) possible

453 differences between dry and wet days (> 1 mm/d), and (b, c) the agreement between remotely

454 sensed and in situ soil moisture measurements from the OBS network using the seasonal

455 classification. To consider any uncertainties arising from spatial averaging, ground

456 measurements are compared to point like and 10x10 km^2 SSM means. The 10x10 km^2 area

457 used covers the OBS area, i.e., the network of in situ measurements within the VAS. For

458 comparison, all grid points from SMOS-L4$^{3.0}$ and SMOS-L2 included within the area are

459 considered.

460 In Figure 7a, the separation between days with and without precipitation (< 1 mm/d) points

461 out similar correlations during dry than wet days (RMSD~0.015, R^2~0.7) for SMOS-L4$^{3.0}$,

462 whereas a slightly better agreement is found for the dry days (not shown) for SMOS-L2. A

463 systematic mean dry bias of about 0.05 (dry days) to 0.08 (wet days) m^3/m^3 is assessed for

464 SMOS-L2, while a lower bias with changing sign is identified for the L4$^{3.0}$ product (~ 0.005

20

465 (wet days); ~ -0.02 (dry days)). Comparisons using the corresponding mean over the 10x10

466 km^2 OBS area, in Figure 7b and Table 3, show good agreement with respect to the SMOS-

467 L4$^{3.0}$ and poorer scores for SMOS-L2 (only one grid point of SMOS-L2 is located within the

468 OBS area). Worse consistency is found in both cases for the MAM and JJA periods. CRMSD

469 is in all cases in the required range of $\leq$ 0.04 m^3/m^3. Point-like comparisons with the

470 individual in situ stations, in Figure 7c and Table 3, show that spatial patterns are captured at

471 1km with RMSD~0.007 to 0.1 m^3/m^3 but, in most cases, accuracy for SMOS-L4$^{3.0}$-1 km

472 disaggregated product is within the required range of less than 0.04 m^3/m^3 (not shown).

473 Higher RMSD is found for SMOS-L2, ~ 0.008 to 0.13 m^3/m^3, accounting for the previously

474 identified dry bias (~ (-0.14) − (-0.02)) reduced in SMOS-L4$^{3.0}$ (~ (-0.08) − (-0.01)). The

475 CRMSD is in all cases $\leq$ 0.04 m^3/m^3. For all stations, better correlations are found in DJF and

476 SON and poorer scores in JJA and MAM, in agreement with the areal-mean comparisons

477 (section 4.1.3). Best scores are obtained for Nicolas, VAS and La Cubera stations, probably in

478 relation to their common soil type distribution, over vineyards, and homogeneous conditions,

479 over a plain (Figure 8a, Table 3). The SON time period reveals the best agreement, at this

480 time the vineyards are completely grown (however, senescent thus containing less water) and

481 SSM exhibits substantial spatial variability driven by precipitation and irrigation thus

482 improving spatio-temporal correlations. Worse statistics are found for Melbex-I, Melbex-II

483 and Ezpeleta, probably in relation to the location of the soil moisture probes in rockier and

484 orographically more complex areas, also in proximity to forestall and man-made construction

485 areas.

486 The soil moisture probability distribution function (PDF; Figure 8b) of all in situ

487 measurements versus SMOS-L4$^{3.0}$ data reveals that the later overestimates SSM below 0.1

488 m^3/m^3, values mainly observed during the JJA period. But, an underestimation occurs in the

489 range between 0.1 and 0.3 m^3/m^3, which is consistent with the identified underestimation of

490   maximum soil moisture reached after a precipitation event and the rapid drying of the soil in

491   comparison to the much slower response seen in the observations during the MAM period

492   (Figure 6c).

493   4.3 SURFEX model simulations and realistic initialization with 1-km soil moisture data

494   4.3.1 SURFEX model simulations of selected stations and realistic initialization

495   As a first step, the performance of the SURFEX(ISBA) SVAT model is evaluated.

496   SURFEX(ISBA) point-like simulations are performed for all in situ soil moisture stations at

497   the VAS area to assess the usefulness of the model for further investigation (Table 4).

498   SURFEX(ISBA) simulations show good agreement with soil moisture ground-based

499   observations at all stations, adequately capturing the associated spatio-temporal variability

500   (slope~1, R^2~ 0.7 to 0.9; MB~0.1 m^3/m^3; CRMSD~0.02 m^3/m^3). It can be concluded that the

501   model performs well and is therefore suitable for further investigation. The seasonal analysis

502   points out the best simulations in the SON period (R^2~0.9 for all stations), but CRMSD is $\leq$

503   0.04 m^3/m^3 for all stations at all periods.

504   Using the mean of the ground-based measurement on the day of the model simulation

505   initialization (realistic initialization; REAL-I)the temporal mean comparison for each station

506   presented in Figure 9 and Table 4 reveals mean R^2~0.8 when the all hydrological year is

507   considered.

508   4.3.2 Spatialization

509   As a first step, point-scale SURFEX-ECMWF and SURFEX-SAFRAN simulations covering

510   the whole investigation period are performed for all in situ soil moisture stations to examine

511   its ability to reproduce soil moisture dynamics. Ground measurements at each station are used

512   for initialization. Scores clearly indicate better agreement with all in situ observations for the

513 SURFEX-SAFRAN simulations (slopes~ 1, R^2~ 0.9, RMSD< 0.1 m^3/m^3), rather than the

514 SURFEX-ECMWF simulations (slopes> 1, R^2~ 0.6, and RMSD> 0.1 m^3/m^3).

515 In a second step, SURFEX-ECMWF and SURFEX-SAFRAN simulations are spatialized to

516 obtain maps of soil moisture over the investigation area. In our CTRL simulations, the daily

517 soil moisture from the mean of the in-situ measurements on the initialization day is used for

518 model initialization. Mean SSM from in situ measurements for the whole investigation period

519 is in the order of 0.14±0.005, whereas SURFEX-ECMWF derived SSM field is about

520 0.18±0.007 and SURFEX-SAFRAN derived SSM field is 0.15±0.002, thus, closer to ground-

521 based observations. Performing a seasonal analysis, we demonstrate that this consistency is

522 maintained for all seasons (not shown). The higher resolution of the SAFRAN-atmospheric

523 forcing better reproduces the high spatial heterogeneity over the VAS area resulting in

524 improved mapping of simulated SSM.

525 Initialization of the SURFEX-SAFRAN simulationusing SMOS-L4[3.0] (EXP-SMOS) is

526 examined against a sensitivity simulation using for the initial soil moisture scenario the

527 climatological soil moisture from observations (daily mean over 10 years, which has been

528 selected to be far from observations; EXP-CLIM). These experiments are initialized in dry

529 periods, following Khodayar et al. (2014) recommendations, to maximize the impact, and run

530 for about 3-4 months. In the first case, initialization is performed in a winter month

531 (December) and the whole simulation period remains almost dry. In the second case, a

532 summer month (July) is chosen for the initialization and it is followed by a wet autumn period

533 with frequent heavy precipitation events in the area.

534 The temporal evolution of the RMSD (Figure 10a) demonstrates that the initial soil moisture

535 scenario influences its evolution until the end of the simulation, in agreement with previous

536 results in section 4.3.1. Larger deviations occur during dry periods, in both scenarios. Longer

537 spin-up times, defined as the time that soil needs to reestablish quasi-equilibrium, characterize

538 the dry scenario. It is after heavy precipitation events that deviations decrease. Soil quickly

539 reacts to changes in the precipitation field in the semi-arid IP. When the upper level soil gets

540 close to saturation soil memory is almost lost. Before the high precipitation events, SSM

541 evolves following the direction of the initial perturbation, i.e., higher initial SSM yields

542 higher SSM, however, a stochastic behaviour is identified afterwards.

543 As an example, differences in the spatial distribution of soil moisture for the winter/dry period

544 simulation are discussed (Figure 10b). A relevant difference in the mean is identified when

545 compared to the CTRL simulation (0.17±0.004): EXP-CLIM (0.014±0.003), EXP_SMOS

546 (0.17±0.003). Clearly, better agreement is found in this last case.

547 Considering the EXP-SMOS initialization scenario simulation, a comparison between

548 simulated point-like and the 10x10 km^2 mean against corresponding ground measurements

549 was done for verification (Figure 10c). Correlations in the order of R^2~0.9 confirm that the

550 combined use of SURFEX-SAFRAN and SMOS-L4$^{3.0}$ for initialization successfully

551 reproduces soil moisture spatial and temporal variability becoming an optimal tool for

552 mapping soil moisture heterogeneity over a study region for diverse purposes.

553

5. Discussion and conclusions

555 High-resolution soil moisture products are essential for our understanding of hydrological and

556 climatic processes as well as improvement of model skills. Due to its high spatial and

557 temporal variability, it is a complicated variable to assess. Mapping high-resolution soil

558 moisture fields using intensively collected in-situ measurements is infeasible. Thus, state of

559 the art high-resolution modelling and satellite-derived products have to fill this gap, although

560 verification is needed. In this study, we examine the potential of the state of the art SMOS-

561 L4$^{3.0}$-1 km "all weather" disaggregated product for assessment of soil moisture variability,

562 and improvement of the SVAT SURFEX(ISBA) simulations, in combination with the

563 SAFRAN meteorological analysis system (SURFEX-SAFRAN), through realistic

564 initialization. A dense network of ground-based soil moisture measurements over the

565 Valencia Anchor Station (VAS; one of the SMOS test sites in Europe) is used for verification.

566 The proposed analysis focuses on the semi-arid IP and covers the one year period of 2012

567 (from December 2011 to December 2012). The comparison of the SMOS-L4$^{3.0}$-1km product

568 to different grid spacing soil moisture data products from SMOS, namely SMOS-L3 (~ 25

569 km) and SMOS-L2 (~15 km) shows that on seasonal time scales SMOS-L4$^{3.0}$ does not

570 accurately capture the spatial variability of the soil moisture field, contrary to SMOS-L3 and

571 SMOS-L2, despite the novelty of introducing ERA-Interim LST data in the MODIS

572 LST/NDVI space (Piles et al. 2014; Sanchez-Ruiz et al. 2014). This is probably in relation to

573 the so different spatial resolution of ERA-Interim and MODIS. This new downscaling

574 approach greatly enhances the potential applicability of the data for those days/periods in

575 which measurements are available, but cannot accurately fill in those periods without

576 measurements dictated by the revisit period of the SMOS satellite, hence, compromising the

577 soil moisture representation as a mean for longer periods than a day. On sub-seasonal time

578 scales, when SMOS images are available, the SMOS-L4$^{3.0}$ high-resolution product shows its

579 potential. It adequately captures the surface soil moisture variability in association with the

580 precipitation field, also when extreme precipitation takes place.

581 Mean and single station comparisons with in-situ measurements reveal that characteristics of

582 SMOS-L4$^{3.0}$ soil moisture fields are closer to in-situ observations than SMOS-L3 and -L2

583 products. Point-like and 10x10 km^2 comparisons show good agreement with respect to the

584 SMOS-L4$^{3.0}$ and poorer scores for SMOS-L2 (e.g. DJF period: SMOS-L3/-L2: Slope:1.1/1.0,

585 R^2:0.5/0.7, Bias:-0.09/(-0.03)). Generally, all three SMOS products adequately reproduce the

586 soil moisture temporal dynamics meeting the desired accuracy of the mission (0.04 m3/m3);

however, the spatial patterns did not always reach the expected precision in agreement with former studies in other regions (Gonzalez-Zamora et al. 2015). Comparisons with ground soil moisture measurements from the eight stations in the OBS network (10×10 km^2) over the VAS area shows that the spatial patterns are captured at 1 km with RMSD~ 0.007 to 0.1 m^3/m^3. The best correlations are in DJF and SON, and poorer scores in MAM and JJA, in agreement with the areal-mean comparisons. SMOS-L4$^{3.0}$ data shows better agreement at those stations over plain areas and with uniform conditions (vineyards), against those over more complex and less homogeneous terrains (rocky soils and areas close to forestall and man-made constructions). The SMOS-L4$^{3.0}$ soil moisture probability distribution function (PDF) in comparison to that of the in-situ measurements reveals a SMOS overestimation below 0.1 m^3/m^3 and an underestimation in the range between 0.1 to 0.3 m^3/m^3. A seasonal analysis points out better scores for the DJF and SON periods, whereas poorer correlation is found for the MAM and JJA periods. In the MAM period, an under-representation of the rainy events is found, as well as faster and stronger drying changes coinciding with the vegetation growth season. In JJA, the very low soil moisture values (< 0.1 m^3/m^3) with associated low spatial variability results in low R^2. No significant differences are found during dry and wet days (> 0.1 mm/d).

SURFEX(ISBA) SVAT simulations covering the whole investigation period over all in-situ measurement stations at the VAS area show good agreement with ground-based observations. Mean values are well reproduced for all stations and the temporal variability is well captured (R2~0.7 to 0.95; RMSD~0.02). The synergetic use of SURFEX(ISBA) simulations with SAFRAN atmospheric forcing information initialized with realistic SSM values from the SMOS-L4$^{3.0}$ data set was successful combination to obtain soil moisture maps over the VAS domain. Good agreement was reached when comparisons between point-like and 10×10 km^2

611   simulations with SURFEX-SAFRAN initialized with SMOS-L4$^{3.0}$ data and in-situ soil

612   moisture measurements were made (R^2~0.9 and RMSD<0.04 m^3/m^3).

613   In this study, the comparison and suitability of different operational satellite products from the

614   SMOS platform is investigated to provide realistic information on the water content of the

615   soil. The comparison carried out helps drawing guidelines on best practices for the sensible

616   use of these products. Currently, there is not a consensus about what is the "best" SMOS

617   product. Different users utilize different products depending on their application rather than

618   based on performance arguments. This study and the conclusions obtained on the comparison

619   are important to provide information on the advantages and drawbacks of these datasets. The

620   high temporal and spatial resolution soil moisture maps obtained in this study could be of use

621   for hydrological and agronomical applications, to build climatologies of SSM, as initial condition

622   for convective system modelling, for flood forecasting and for downstream local applications

623   such as crop monitoring and crop development strategies as well as for irrigation data sets,

624   among others. Additionally, an accurate representation of SSM will permit the calculation of

625   SM profiles by application of e.g. exponential filters, which has been demonstrated to be a

626   successful technique. Furthermore, the added value of the SMOS-L4$^{3.0}$-1 km disaggregated

627   product for initialization purposes is demonstrated, which suggests its potential for

628   assimilation purposes. These two last aspects are out of the scope of theispaper, but they are

629   investigated in detail in a follow-up study. Important aspects of the SMOS-L4$^{3.0}$ SSM product

630   have still to be improved, namely its temporal availability (e.g. successful investigations on

631   the increase of SMOS-L3 temporal resolution to 3h are available (Louvet et al. 2015)), its

632   spatio-temporal correlation with in situ measurements over complex topographic areas, in

633   areas/periods with low spatial variability and in rainy periods when an under-representation

634   and rapid decay of SSM has been identified.

635

636 **Acknowledgements**

649

650

651

652

653

654

655

656

657 **References**

658 ARRAY Systems Computing Inc., CESBIO, IPSL-Service d'Aéronomie, INRA-EPHYSE,

659 Reading University, Tor Vergata University. Algorithm Theoretical Basis Document (ATBD)

660 for the SMOS Level 2 Soil Moisture Processor Development Continuation Project. ESA No.:

661 SO-TN-ARR-L2PP-0037 Issue: 3.9 Array No.: ASC_SMPPD_037 Date: October 24, 2014

662

663 Bircher, S., Skou, N., Jensen, K. H., Walker, J. P., & Rasmussen, L. (2012). A soil moisture

664 and temperature network for SMOS validation in Western Denmark. Hydrology and Earth

665 System Sciences, 16(5), 1445-1463.

666

667 Bolle, H.-J., Eckardt, M., Koslowsky, D., Maselli, F., Meliá Miralles, J., Menenti, M., Olesen,

668 F.-S., Petkov, L., Rasool, I., Van de Griend, A.A. (Editors). Contributing Authors: H. Billing,

669 A. Gitelson, F. Göttsche, A. Jochum-Osann, E. Lopez-Baeza, F. Meneguzzo, J. Moreno, F.

670 Nerry, P. Rossini, F. Veroustraete, R. Vogt, P.J. Van Oeleven. Mediterranean Landsurface

671 Processes Assessed From Space. Chapter 6 From Research to Application. Regional Climate

672 Studies Series. Springer-Verlag Berlin Heidelberg, ISBN: 978-3-540-40151-3 (Print) 978-3-

673 540-45310-9 (Online) (2006)

674

675 Boone, A., Calvet, J.-C., & Noilhan, J. (1999). Inclusion of a Third Soil Layer in a Land

676 Surface Scheme Using the Force–Restore Method. Journal of Applied Meteorology, 38,

677 1611−1630. https://doi.org/10.1175/1520-0450(1999)038<1611:IOATSL>2.0.CO;2

678   Bosch, D. D., J. M. Sheridan, and L. K. Marshall (2007), Precipitation, soil moisture, and

679   climate database, Little River Experimental Watershed, Georgia, United States, Water Resour.

680   Res., 43, W09472, doi:10.1029/2006WR005834

681

682   Brocca, L., Melone, F., Moramarco, T., Wagner, W., & Hasenauer, S. (2010). ASCAT soil

683   wetness index validation through in situ and modeled soil moisture data in central Italy.

684   Remote Sensing of Environment, 114(11), 2745-2755.

685

686   Calvet, J.-C., Noilhan, J., & Bessemoulin, P. (1998). Retrieving the Root-Zone Soil Moisture

687   from Surface Soil Moisture or Temperature Estimates: A Feasibility Study Based on Field

688   Measurements.   Journal   of   Applied   Meteorology,   37(1995),   371–386.

689   https://doi.org/10.1175/1520-0450(1998)037<0371:RTRZSM>2.0.CO;2

690

691   Clapp, R. B., & Hornberger, G. M. (1978). Empirical equations for some soil hydraulic

692   properties. Water resources research, 14(4), 601-604.

693

694   Cosby, B. J., Hornberger, G. M., Clapp, R. B., & Ginn, T. (1984). A statistical exploration of

695   the relationships of soil moisture characteristics to the physical properties of soils. Water

696   resources research, 20(6), 682-690.

697

698 Cosh, M. H., Jackson, T. J., Bindlish, R., & Prueger, J. H. (2004). Watershed scale temporal

699 and spatial stability of soil moisture and its role in validating satellite estimates. Remote

700 sensing of Environment, 92(4), 427-435.

701

702 Djamai, N., Magagi, R., Goïta, K., Merlin, O., Kerr, Y., Roy, A. (2016). A combination of

703 DISPATCH downscaling algorithm with CLASS land surface scheme for soil moisture

704 estimation at fine scale during cloudy days. Remote Sensing of Environment, 184, 1-14.

705

706 De Lannoy, G. J., & Reichle, R. H. (2016). Global assimilation of multiangle and

707 multipolarization SMOS brightness temperature observations into the GEOS-5 catchment

708 land surface model for soil moisture estimation. Journal of Hydrometeorology, 17(2), 669-

709 691.

710

711 Delwart, S., Bouzinac, C., Wursteisen, P., Berger, M., Drinkwater, M., Martín-Neira, M., &

712 Kerr, Y. H. (2008). SMOS validation and the COSMOS campaigns. IEEE Transactions on

713 Geoscience and Remote Sensing, 46(3), 695-704.

714

715 Dente, L., Su, Z., & Wen, J. (2012). Validation of SMOS soil moisture products over the

716 Maqu and Twente regions. Sensors, 12(8), 9965-9986.

717

718 Drobinski P., V. Ducrocq, P. Alpert, E. Anagnostou, K. Béranger, M. Borga, I. Braud, A.

719 Chanzy, S. Davolio, G. Delrieu, C. Estournel, N. Filali Boubrahmi, J. Font, V. Grubišić, S.

720 Gualdi, V. Homar, B. Ivančan-Picek, C. Kottmeier, V. Kotroni, K. Lagouvardos, P. Lionello,

721 M. C. Llasat, W. Ludwig, C. Lutoff, A. Mariotti, E. Richard, R. Romero, R. Rotunno, O.

722 Roussot, I. Ruin, S. Somot, I. Taupier-Letage, J. Tintore, R. Uijlenhoet, and H. Wernli, 2014.

723 HyMeX: A 10-year multidisciplinary program on the Mediterranean water cycle. Bull. Amer.

724 Meteor. Soc., 95, 1063–1082. doi: http://dx.doi.org/10.1175/BAMS-D-12-00242.1

725

726 Ducrocq Véronique, Isabelle Braud, Silvio Davolio, Rossella Ferretti, Cyrille Flamant,

727 Agustin Jansa, Norbert Kalthoff, Evelyne Richard, Isabelle Taupier-Letage, Pierre-Alain

728 Ayral, Sophie Belamari, Alexis Berne, Marco Borga, Brice Boudevillain, Olivier Bock, Jean-

729 Luc Boichard, Marie-Noëlle Bouin, Olivier Bousquet, Christophe Bouvier, Jacopo Chiggiato,

730 Domenico Cimini, Ulrich Corsmeier, Laurent Coppola, Philippe Cocquerez, Eric Defer,

731 Julien Delanoë, Paolo Di Girolamo, Alexis Doerenbecher, Philippe Drobinski, Yann

732 Dufournet, Nadia Fourrié, Jonathan J. Gourley, Laurent Labatut, Dominique Lambert, Jérôme

733 Le Coz, Frank S. Marzano, Gilles Molinié, Andrea Montani, Guillaume Nord, Mathieu Nuret,

734 Karim Ramage, William Rison, Odile Roussot, Frédérique Said, Alfons Schwarzenboeck,

735 Pierre Testor, Joël Van Baelen, Béatrice Vincendon, Montserrat Aran, and Jorge Tamayo,

736 2014. HyMeX-SOP1: The field campaign dedicated to heavy precipitation and flash flooding

737 in the Northwestern Mediterranean. Bull. Amer. Meteor. Soc., 95, 1083–1100. doi:

738 http://dx.doi.org/10.1175/BAMS-D-12-00244.1

739

740 Duffourg, F., & Ducrocq, V. (2011). Origin of the moisture feeding the Heavy Precipitating

741 Systems over Southeastern France. Natural Hazards and Earth System Sciences, 11(4), 1163.

742

743   Duffourg, F., & Ducrocq, V. (2013). Assessment of the water supply to Mediterranean heavy

744   precipitation: a method based on finely designed water budgets. Atmospheric Science Letters,

745   14(3), 133-138.

746

747   Durand, Y., E. Brun, L. Mérindol, G. Guyomarc'h, B. Lesaffre, E. Martin, A meteorological

748   estimation of relevant parameters for snow models, Ann. Glaciol. 18 (1993) 65–71.

749

750   Durand, Y., G. Giraud, M. Laternser, P. Etchevers, L. Mérindol, B. Lesaffre, Reanalysis of 47

751   Years of Climate in the French Alps (1958–2005): Climatology and Trends for Snow Cover,

752   J. Appl. Meteorol. Climatol. 48 (2009) 2487–2512.

753   Entekhabi, D., Rodriguez-Iturbe, I., & Castelli, F. (1996). Mutual interaction of soil moisture

754   state and atmospheric processes. Journal of Hydrology, 184(1-2), 3-17.

755

756   Entekhabi, D.; Njoku, E.G.; Neill, P.E.; Kellogg, K.H.; Crow, W.T.; Edelstein,W.N.; Entin,

757   J.K.; Goodman, S.D.; Jackson, T.J.; Johnson, J. The soil moisture active passive (SMAP)

758   mission (2010). Proc. IEEE, 98, 704–716.

759   FAO; World reference base for soil resources 2014 international soil classification system for

760   naming soils and creating legends for soil maps. Rome: FAO, 2014.

761

762   Gherboudj, I., Magagi, R., Goïta, K., Berg, A. A., Toth, B., & Walker, A. (2012). Validation

763   of SMOS data over agricultural and boreal forest areas in Canada. IEEE Transactions on

764   Geoscience and Remote Sensing, 50(5), 1623-1635.

765

766 GTOPO30 Documentation, U.S. Geological Survey, 1996, Global 30 Arc-Second Elevation

767 A. Gonzalez-Zamora, N. Sánchez, J. Martinez-Fernandez, A. Gumuzzio, M. Piles, E.

768 Olmedo. Long-Term SMOS Soil Moisture Products: A Comprehensive Evaluation across

769 Scales and Methods in the Duero Basin Physics and Chemistry of the Earth, Parts A/B/C, 83–

770 84 (2015), pp. 123–136 http://dx.doi.org/10.1016/j.pce.2015.05.009

771

772 Hirschi, M., Seneviratne, S. I., Alexandrov, V., Boberg, F., Boroneant, C., Christensen, O. B.,

773 and Stepanek, P. (2011). Observational evidence for soil-moisture impact on hot extremes in

774 southeastern Europe. Nature Geoscience, 4(1), 17.

775

776 Jansa, J., Erb, A., Oberholzer, H. R., Šmilauer, P., & Egli, S. (2014). Soil and geography are

777 more important determinants of indigenous arbuscular mycorrhizal communities than

778 management practices in Swiss agricultural soils. Molecular ecology, 23(8), 2118-2135.

779

780 Jones, M. O., L. A. Jones, J. S. Kimball, and K. C. McDonald (2011), Satellite passive

781 microwave remote sensing for monitoring global land surface phenology, Remote Sens.

782 Environ., 115(4), 1102–1114, doi:10.1016/j.rse.2010.12.015.

783

784 Juglea, S., Kerr, Y., Mialon, A., Lopez-Baeza, E., Braithwaite, D., & Hsu, K. (2010). Soil

785 moisture modelling of a SMOS pixel: Interest of using the PERSIANN database over the

786 Valencia Anchor Station. Hydrology and Earth System Sciences, 14(8), 1509–1525.

787 https://doi.org/10.5194/hess-14-1509-2010

788

789 Juglea, S., Kerr, Y., Mialon, A., Wigneron, J. P., Lopez-Baeza, E., Cano, A., … Delwart, S.

790 (2010). Modelling soil moisture at SMOS scale by use of a SVAT model over the Valencia

791 Anchor Station. Hydrology and Earth System Sciences, 14(5), 831–846.

792 https://doi.org/10.5194/hess-14-831-2010

793

794 Kerr, Y. H. (2007). Soil moisture from space: Where are we?. Hydrogeology journal, 15(1),

795 117-120.

796

797 Kerr, Y. H., Waldteufel, P., Wigneron, J. P., Delwart, S., Cabot, F., Boutin, J., ... & Juglea, S.

798 E. (2010). The SMOS mission: New tool for monitoring key elements ofthe global water

799 cycle. Proceedings of the IEEE, 98(5), 666-687.

800

801 Kerr, Y. H., Waldteufel, P., Wigneron, J. P., Martinuzzi, J. A. M. J., Font, J., & Berger, M.

802 (2001). Soil moisture retrieval from space: The Soil Moisture and Ocean Salinity (SMOS)

803 mission. IEEE transactions on Geoscience and remote sensing, 39(8), 1729-1735.

804

805 Khodayar, S., Raff, F., Kalthoff, N. 2015. Dignostic Study of a High Precipitation Event   in

806 the Western Mediterranean Region: Adequacy of Current operational Networks

807 Quart. J. Roy. Meteor. Soc. DOI: 10.1002/qj.2600

808

809 Khodayar, S., Sehlinger, A., Feldmann, H., & Kottmeier, C. (2015). Sensitivity of soil

810 moisture initialization for decadal predictions under different regional climatic conditions in

811 Europe. International Journal of Climatology, 35(8), 1899-1915.

812

813 Koster, R. D., Dirmeyer, P. A., Guo, Z., Bonan, G., Chan, E., Cox, P., ... & Liu, P. (2004).

814 Regions of strong coupling between soil moisture and precipitation. Science, 305(5687),

815 1138-1140.

816

817 Le Moigne, P., Boone, A., Calvet, J. C., Decharme, B., Faroux, S., Gibelin, A. L., ... &

818 Mironov, D. (2009). SURFEX scientific documentation. Note de centre (CNRM/GMME),

819 Météo-France, Toulouse, France.

820

821 Liu, Y.Y.; Parinussa, R.M.; Dorigo, W.A.; De Jeu, R.A.M.; Wagner, W.; van Dijk, A.I.J.M.;

822 McCabe, M.F.; Evans, J.P. Developing an improved soil moisture dataset by blending passive

823 and active microwave satellite-based retrievals (2011). Hydrol. Earth Syst. Sci., 15, 425–436.

824

825 Louvet, S., Thierry Pellarin, Ahmad al Bitar, Bernard Cappelaere, Sylvie Galle, Manuela

826 Grippa, Claire Gruhier, Yann Kerr, Thierry Lebel, Arnaud Mialon, Eric Mougin, Guillaume

827 Quantin, Philippe Richaume, Patricia de Rosnay (2015). SMOS soil moisture product

828 evaluation over West-Africa from local to regional scale. Remote Sensing of Environment,

829 Volume 156, Pages 383-394, ISSN 0034-4257, DOI: 10.1016/j.rse.2014.10.005.

830

831   Malbéteau, Y., Merlin, O., Balsamo, G., Er-Raki, S., Khabba, S.,Walker, J. P., Jarlan, L.

832   (2018). Toward a Surface Soil Moisture Product at High Spatiotemporal Resolution:

833   Temporally Interpolated, Spatially Disaggregated SMOS Data. Journal of Hydrometeorology,

834   19(1), 183-200.

835

836   Masson, V., Champeaux, J. L., Chauvin, F., Meriguet, C., & Lacaze, R. (2003). A global

837   database of land surface parameters at 1-km resolution in meteorological and climate models.

838   Journal of Climate, 16(9), 1261–1282. https://doi.org/10.1175/1520-0442-16.9.1261

839

840   Merlin, O., Rüdiger, C., Al Bitar, A., Richaume, P., Walker, J. P., & Kerr, Y. H. (2012).

841   Disaggregation of SMOS soil moisture in Southeastern Australia. IEEE Transactions on

842   Geoscience and Remote Sensing, 50(5), 1556–1571. http://dx.doi.org/10.1109/TGRS.

843   2011.2175000.

844   Naeimi, V.; Scipal, K.; Bartalis, Z.; Hasenauer, S.; Wagner, W. An improved soil moisture

845   retrieval algorithm for ers and metop scatterometer observations (2009). IEEE Trans. Geosci.

846   Remote Sens. 47, 1999–2013.

847

848   Noilhan, J., & Planton, S. (1989). A Simple Parameterization of Land Surface Processes for

849   Meteorological Models. Monthly Weather Review. https://doi.org/10.1175/1520-

850   0493(1989)117<0536:ASPOLS>2.0.CO;2

851   Owe, M.; de Jeu, R.; Holmes, T. Multisensor historical climatology of satellite-derived global

852   land surface moisture (2008). J. Geophys. Res. Earth Surf., 113, F01002.

853

854   Piles, M., Camps, A., Vall-Llossera, M., Corbella, I., Panciera, R., Rudiger, C., … Walker, J.

855   (2011). Downscaling SMOS-derived soil moisture using MODIS visible/infrared data. IEEE

856   Transactions   on   Geoscience   and   Remote   Sensing,   49(9),   3156–3166.

857   https://doi.org/10.1109/TGRS.2011.2120615

858

859   Piles, M., Sánchez, N., Vall-Llossera, M., Camps, A., Martínez-Fernandez, J., Martinez, J., &

860   Gonzalez-Gambau, V. (2014). A downscaling approach for SMOS land observations:

861   Evaluation of high-resolution soil moisture maps over the Iberian peninsula. IEEE Journal of

862   Selected Topics in Applied Earth Observations and Remote Sensing, 7(9), 3845–3857.

863   https://doi.org/10.1109/JSTARS.2014.2325398

864

865   Piles, M., Vall-Llossera, M., Camps, A., Sanchez, N., Martinez-Fernandez, J., Martinez, J., …

866   Riera, R. (2013). On the synergy of SMOS and Terra/Aqua MODIS: High resolution soil

867   moisture maps in near real-time. International Geoscience and Remote Sensing Symposium

868   (IGARSS), 3423–3426. https://doi.org/10.1109/IGARSS.2013.6723564

869

870   Piles, M., Pou, X., Camps, A., Vall-llosera, M. (2015): Quality report: Validation of SMOS-

871   BEC L4 high resolution soil moisture products, version 3.0 or "all-weather". Technical report.

872   Available at: http://bec.icm.csic.es/doc/BEC-SMOS-L4SMv3-QR.pdf

873

874   Quintana-Segui, P., Le Moigne, P., Durand, Y., Martin, E., Habets, F., Baillon, M., ... &

875   Morel, S. (2008). Analysis of near-surface atmospheric variables: Validation of the SAFRAN

876   analysis over France. Journal of applied meteorology and climatology, 47(1), 92-107.

877

878   Quintana-Seguí, P., Peral, C., Turco, M., Llasat, M. C., & Martin, E. (2016). Meteorological

879   Analysis Systems in North-East Spain: Validation of SAFRAN and SPAN. Journal of

880   Environmental Informatics, 27(2).

881

882   Raveh-Rubin, S., and Wernli, H. (2015). Large-scale wind and precipitation extremes in the

883   Mediterranean: a climatological analysis for 1979–2012. Quarterly Journal of the Royal

884   Meteorological Society, 141(691), 2404-2417.

885

886   Robock, A., Vinnikov, K. Y., Srinivasan, G., Entin, J. K., Hollinger, S. E., Speranskaya, N.

887   A., ... & Namkhai, A. (2000). The global soil moisture data bank. Bulletin of the American

888   Meteorological Society, 81(6), 1281-1299.

889

890   Rosenbaum, U., H. R. Bogena, M. Herbst, J. A. Huisman, T. J. Peterson, A. Weuthen, A. W.

891   Western, and H. Vereecken (2012), Seasonal and event dynamics of spatial soil moisture

892   patterns at the small catchment scale, WaterResour.Res., 48, W10544,

893   doi:10.1029/2011WR011518.

894

895   Sanchez N., J. Martinez-Fernandez, A. Scaini and C. Perez-Gutierrez, "Validation of the

896   SMOS L2 Soil Moisture Data in the REMEDHUS Network (Spain)," in IEEE Transactions

897   on Geoscience and Remote Sensing, vol. 50, no. 5, pp. 1602-1611, May 2012. doi:

898   10.1109/TGRS.2012.2186971

899

900   Sánchez-Ruiz, S., Piles, M., Sánchez, N., Martínez-Fernández, J., Vall-llossera, M., &

901   Camps, A. (2014). Combining SMOS with visible and near/shortwave/thermal infrared

902   satellite data for high resolution soil moisture estimates. Journal of Hydrology, 516, 273–283.

903   https://doi.org/10.1016/j.jhydrol.2013.12.047

904

905   Schubert, M., & Boche, H. (2004). Solution of the multiuser downlink beamforming problem

906   with individual SINR constraints. IEEE Transactions on Vehicular Technology, 53(1), 18-28.

907

908   Schwank, M., Wigneron, J. P., Lopez-Baeza, E., Volksch, I., Matzler, C., & Kerr, Y. H.

909   (2012). L-band radiative properties of vine vegetation at the MELBEX III SMOS cal/val site.

910   IEEE Transactions on Geoscience and Remote Sensing, 50(5), 1587-1601.

911

912   Seneviratne, S. I., Corti, T., Davin, E. L., Hirschi, M., Jaeger, E. B., Lehner, I., ... & Teuling,

913   A. J. (2010). Investigating soil moisture–climate interactions in a changing climate: A review.

914   Earth-Science Reviews, 99(3), 125-161.

915

916   SMOS-BEC Team (2016): SMOS-BEC Ocean and Land Products Description. Technical

917   report. Available at: http://bec.icm.csic.es/doc/BEC-SMOS-0001-PD.pdf

918

919   Taylor, C. M., & Lebel, T. (1998). Observational evidence of persistent convective-scale

920   rainfall patterns. Monthly Weather Review, 126(6), 1597-1607.

921

922   Vautard, R., Yiou, P., D'andrea, F., De Noblet, N., Viovy, N., Cassou, C., ... & Fan, Y.

923   (2007). Summertime European heat and drought waves induced by wintertime Mediterranean

924   rainfall deficit. Geophysical Research Letters, 34(7).

925

926   Vidal, J.-P., E. Martin, L. Franchistéguy, M. Baillon, J.-M. Soubeyroux, A 50-year high-

927   resolution atmospheric reanalysis over France with the Safran system, Int. J. Climatol. 30

928   (2010) 1627–1644.

929

930   Wagner, W.; Dorigo, W.; de Jeu, R.; Fernandez, D.; Benveniste, J.; Haas, E.; Ertl, M. Fusion

931   of active and passive microwave observations to create an essential climate variable data

932   record on soil moisture (2012). ISPRS Ann. Photogramm. Remote Sens. Spat. Inf. Sci. 1–7,

933   315–321.

934

935   Walker, J., & Rowntree, P. R. (1977). The effect of soil moisture on circulation and rainfall in

936   a tropical model. Quarterly Journal of the Royal Meteorological Society, 103(435), 29-46.

937

938   Western, A. W., Grayson, R. B., & Blöschl, G. (2002). Scaling of soil moisture: A hydrologic

939   perspective. Annual Review of Earth and Planetary Sciences, 30(1), 149-180.

940

941   Wigneron, J. P., Calvet, J. C., Pellarin, T., Van de Griend, A. A., Berger, M., & Ferrazzoli, P.

942   (2003). Retrieving near-surface soil moisture from microwave radiometric observations:

943   current status and future plans. Remote Sensing of Environment, 85(4), 489-506.

944

945   Wigneron, J.-P., M. Schwank, E. Lopez Baeza, Y. Kerr, N. Novello, C. Millan, C. Moisy, P.

946   Richaume, A. Mialon, A. Al Bitar, F. Cabot, H. Lawrence, D. Guyon, J-C Calvet, J. P. Grant,

947   P. de Rosnay, A. Mahmoodi, S. Delwart, S. Mecklenburg (2012). First Evaluation of the

948   Simultaneous SMOS and ELBARA-II Observations in the Mediterranean Region. Remote

949   Sensing of Environment, 124, 26–37

950

951   Zampieri, M., F. D'Andrea, R. Vautard, P. Ciais, N. de Noblet-Ducoudré, and P. Yiou, 2009:

952   Hot European Summers and the Role of Soil Moisture in the Propagation of Mediterranean

953   Drought. J. Climate, 22, 4747–4758, https://doi.org/10.1175/2009JCLI2568.1

954

955

956

957

958

959

960

961

962 **Tables**

963

964 **Table 1:** Characteristics of soil moisture stations within the VAS domain.

NAME	STATION	DOMINANT VEGETATION USED FOR SIMULATIONS	TYPE OF VEGETATION	SAND	SILT	CLAY	ALTITUDE (m)	ANNUAL MEAN TEMPERATURE (°C)	ANNUAL MEAN PRECIPITATION (mm)
Melbex_I		Schrub	Schrub	0,47	0,38	0,15	849		
Nicolas		Vineyard	Schrub/ Vineyard	0,47	0,35	0,18	859		
La Cubera		Vineyard	Vineyard	0,45	0,35	0,20	762	(12-14)	451
Ezpeleta		Olive tree	Olive tree	0,44	0,39	0,17	781		
VAS		Vineyard	Vineyard	0,46	0,37	0,17	804		
Melbex_II		Vineyard	Vine stump/ Vine row	0,45	0,29	0,26	797		

965

966

967

968

969

970

971

972

973

974

975

976

977

978

979

980

981

982 **Table 2:** Number of days (percentage) in which the SMOS (ascendant and descendent
983 swaths) coverage is higher than 50 %.

984

LEVEL SMOS	SEPTEMBER		OCTOBER		NOVEMBER		SON	
	days	%	days	%	days	%	days	%
L4$^{2.0}$ (~1km)	10	34	9	31	9	31	28	32
L4$^{3.0}$ (~1km)	23	74	29	90	30	100	82	92
L2 (~15km)	20	67	28	90	28	93	76	83
L3 (~25km)	22	73	29	93	29	96	80	88

985

986

987

988

989

990

991

992

993

994

995

996

997

998

999

1000

1001

1002

1003

1004

1005 **Table 3:** Statistics of the comparions between SMOS-L2 and SMOS-L4$^{3.0}$ soil moisture
1006 versus ground-based measurements in the VAS network (the area covering the ground-
1007 based network has been called OBS, Figure 1). SMOS descendent orbits are selected for
1008 the comparison. Characteristics of the individual stations are given in Table 1. The acronyms
1009 for the names of the stations are as follows: (M-I: Melbex_I, M_II: Melbex_II, VAS: VAS, NIC:
1010 Nicolas, EZ: Ezpeleta, LC: La Cubera). The period December 2011 to December 2012 is
1011 evaluated. The seasonal analysis follows the hydrological cycle. OBS stands for the average
1012 of (i) SMOS-L2 and/or SMOS-L4$^{3.0}$ soil moisture values within the 10x10 km^2 where the
1013 ground-based network is placed, and (ii) in the case of the in situ observations it refers to the
1014 mean of all stations. In Table (a) a seasonal comparison between the mean of all in situ
1015 stations and the corresponding mean of SMOS-L2 and/or SMOS-L4$^{3.0}$ soil moisture values
1016 within the 10x10 km^2 area. In (b) SMOS-L2 and SMOS-L4$^{3.0}$ soil moisture observations are
1017 compared to point-like ground measurements using the closest grid point. The column on the
1018 right shows the mean of all stations

1019

1020 (a)

OBS vs SMOS-L2	Slope	R2	Bias	CRMS	OBS vs SMOS-L4$^{3.0}$	Slope	R2	Bias	CRMS
DJF	1.1	0.5	-0.09	0.03	DJF	1.0	0.7	-0.03	0.04
MAM	0.6	0.2	-0.07	0.03	MAM	0.6	0.4	-0.03	0.03
JJA	0.3	0.01	-0.02	0.03	JJA	0.1	0.01	-0.003	0.03
SON	1.1	0.8	-0.02	0.04	SON	0.8	0.7	-0.003	0.04

1021

1022 (b)

SMOSL2 vs SMOSL4$^{3.0}$	M-I	M-II	VAS	NIC	EZ	LC	OBS (mean all stations)
DJF							
Slope	0.17/-0.04	1.0/1.7	1.6/2.3	1.1/1.7	0.8/0.9	0.9/1.7	1.1/0.6
R2	0.02/0.01	0.6/0.5	0.8/0.5	0.9/0.7	0.5/0.2	0.7/0.7	0.5/0.7
MB	-0.03/-0.08	-0.08/-0.14	0.01/-0.04	0.006/-0.05	0.03/-0.02	0.004/-0.05	-0.09/-0.03
CRMSD	0.04/0.03	0.03/0.02	0.04/0.03	0.03/0.03	0.04/0.03	0.04/0.03	0.03/0.04
MAM							
Slope	0.4/0.36	0.6/0.4	0.8/0.6	0.6/0.8	0.5/0.3	0.9/0.7	0.6/0.6
R2	0.2/0.08	0.3/0.04	0.5/0.15	0.9/0.5	0.3/0.14	0.4/0.2	0.2/0.4
MB	-0.04/-0.08	-0.08/-0.11	0.005/-0.03	0.003/-0.03	0.02/-0.02	-0.02/-0.05	-0.07/-0.03
CRMSD	0.03/0.03	0.03/0.03	0.03/0.03	0.03/0.03	0.04/0.03	0.03/0.03	0.03/0.03
JJA							
Slope	0.26/0.38	0.3/0.4	0.02/0.15	0.1/0.3	0.08/-0.04	0.05/0.06	0.3/0.1
R2	0.02/0.01	0.04/0.005	0.001/0.002	0.8/0.17	0.003/0.012	0.01/0.003	0.01/0.01
MB	-0.01/-0.03	-0.04/-0.05	0.03/0.012	0.01/0.002	0.05/0.04	0.03/0.02	-0.02/-0.003
CRMSD	0.03/0.03	0.03/0.03	0.03/0.03	0.03/0.03	0.03/0.03	0.03/0.03	0.03/0.03
SON							
Slope	0.69/1.06	0.9/1.3	1.2/1.7	0.8/1.2	0.7/1.1	0.8/1.3	1.1/0.8
R2	0.5/0.6	0.6/0.6	0.7/0.8	0.9/0.7	0.8/0.7	0.8/0.7	0.8/0.07
MB	-0.02/-0.04	-0.03/-0.05	0.04/-0.03	0.03/0.006	0.03/0.01	0.04/0.02	-0.02/-0.003
CRMSD	0.04/0.04	0.04/0.04	0.04/0.04	0.04/0.04	0.04/0.04	0.04/0.04	0.04/0.04

1023

1024

1025

1026

1027

1028

1029

1030

1031 **Table 4:** Statistics of daily areal averages of ground-based SSM measurements in the OBS
1032 area versus point-like SURFEX(ISBA) simulations at the same sites. The acronyms for the
1033 names of the stations are as described in Table 3.

1034

	M-I	M-II	VAS	NIC	EZ	LC	OBS
All period							
Slope	0.9	1.3	0.9	0.7	1.0	0.9	1.0
R2	0.8	0.8	0.8	0.8	0.8	0.7	0.9
MB	0.004	-0.012	0.011	0.006	0.02	0.006	0.005
CRMSD	0.02	0.02	0.02	0.02	0.01	0.02	0.02
DJF							
Slope	0.2	1.3	0.8	1.2	1.2	1.1	1.1
R2	0.03	0.4	0.4	0.7	0.7	0.5	0.6
MB	0.01	-0.03	0.02	0.03	0.02	0.03	0.01
CRMSD	0.04	0.05	0.03	0.04	0.03	0.03	0.04
MAM							
Slope	0.8	1.0	1.0	0.7	0.8	0.7	0.9
R2	0.5	0.4	0.6	0.4	0.6	0.5	0.6
MB	0.002	-0.02	0	0.01	0.01	-0.02	-0.004
CRMSD	0.04	0.02	0.03	0.04	0.03	0.04	0.04
JJA							
Slope	0.4	0.8	1.6	3	1.6	2	1.5
R2	0.7	0.8	0.7	0.5	0.7	0.6	0.8
MB	0.004	0.01	0.01	-0.02	0.02	0.005	0.005
CRMSD	0.04	0.02	0.03	0.04	0.03	0.04	0.04
SON							
Slope	0.9	1.1	0.9	0.8	1.0	1.1	1.0
R2	0.8	0.8	0.8	0.9	0.9	0.8	0.9
MB	0.002	0	0.01	0	0.02	0.01	0.006
CRMSD	0.04	0.006	0.03	0.04	0.04	0.03	0.04

1035

1036

1037

1038

1039

1040

1041

1042

1043

1044

1045

1046

1047 **Figures**

1048
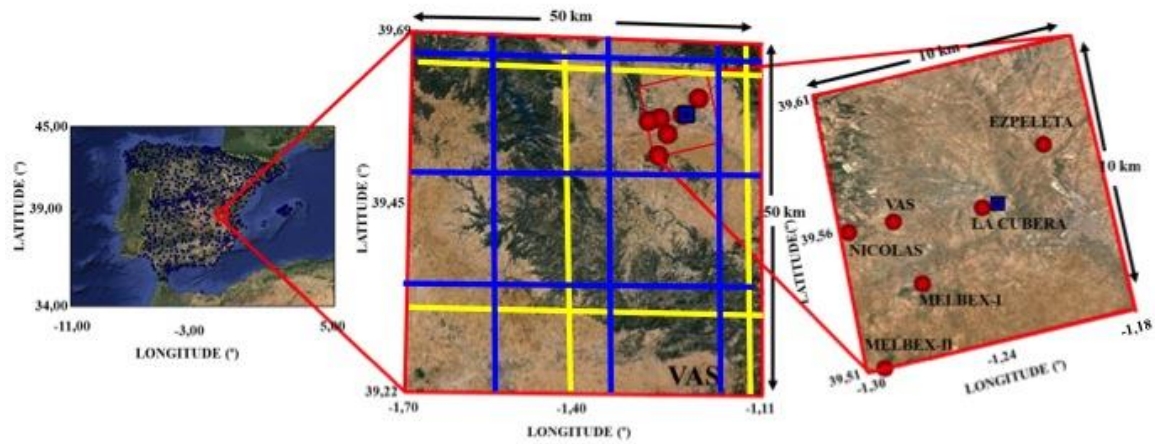
1049

1050

1051 **Figure 1:** Area of investigation and orography. Location of rain gauges from AEMET
1052 (Meteorological Service of Spain) is shown over the Iberian Peninsula (blue square dots).
1053 The positions of the soil moisture network stations within the 10x10 km^2 (OBS area) in the
1054 Valencia Anchor Station (VAS; 50x50 km^2) area are indicated by red circles.

1055

1056

1057

1058

1059

1060

1061

1062

1063

1064

1065

1066
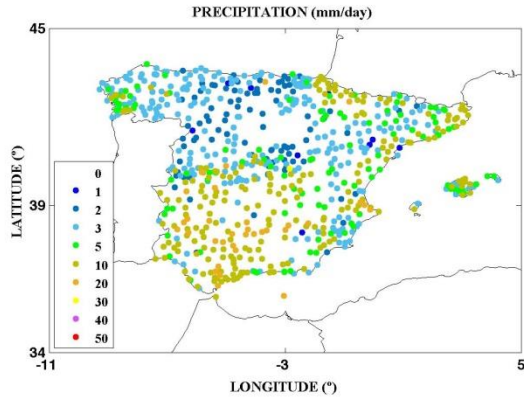
1067
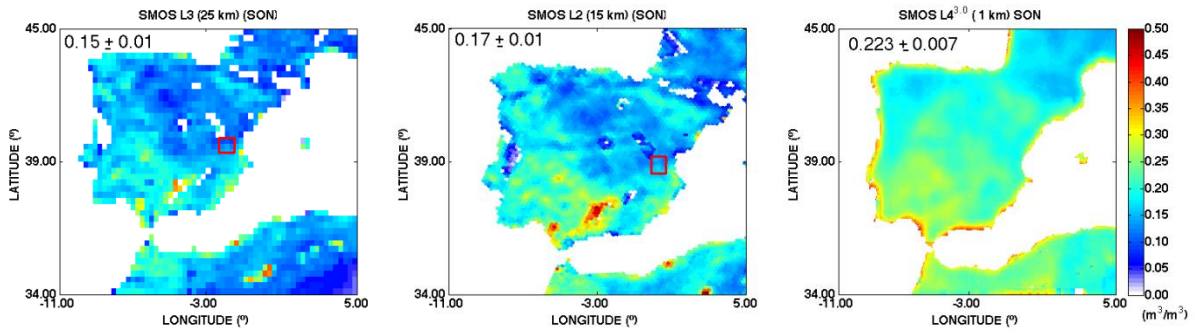
1068
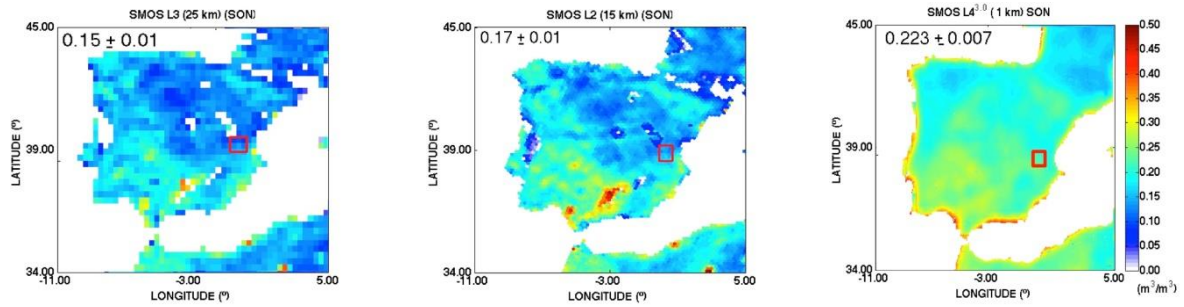
1069

1070

Figure 2: (a) Spatial distribution of precipitation over the Iberian Peninsula from the network of rain gauges of AEMET. The period of September to November (SON) 2012 is shown. (b) Spatial distribution of SMOS-derived soil moisture over the Iberian Peninsula (merged product: ascending and descending orbits, days with areal coverage higher than 50 % are considered).

1076

1077

1078

1079

1080

1081

1082

1083

1084

1085

1086

1087

1088
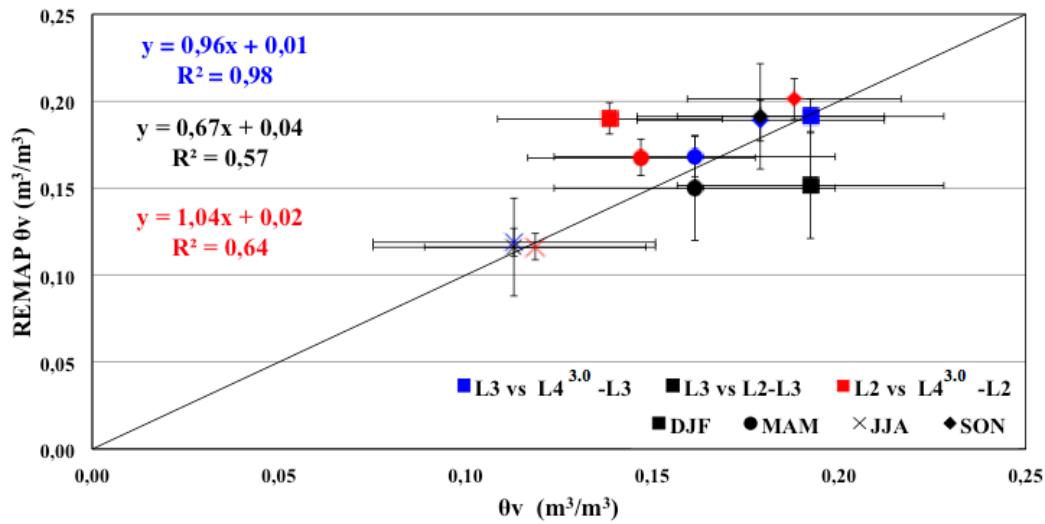
1089

1090

1091 **Figure 3:** SMOS-derived SSM products comparison from different operational levels over the
1092 Iberian Peninsula.

1093

1094

1095

1096

1097

1098

1099

1100

1101

1102

1103

1104

1105   (a)
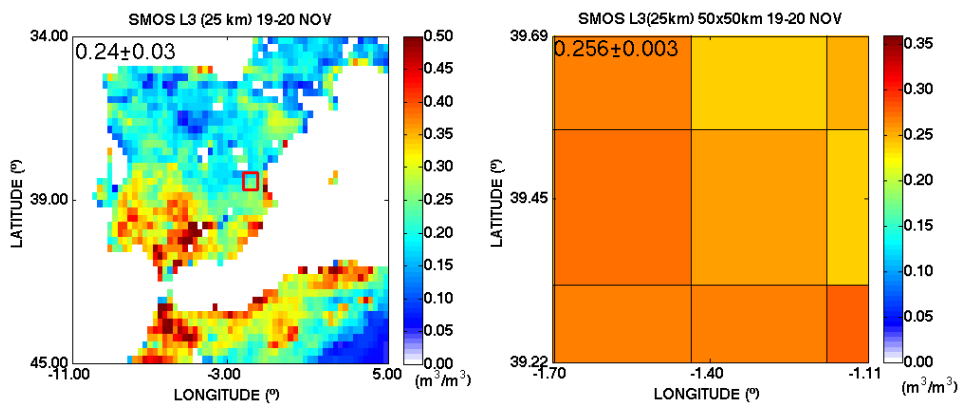
1106
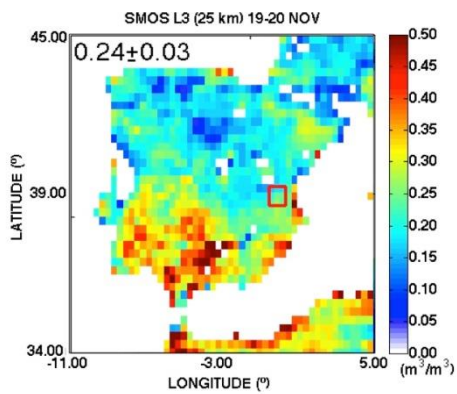
1107

1108

1109

1110

1111

1112

1113

1114

1115

1116

1117

1118

1119

1120

1121

1122

1123   (b)
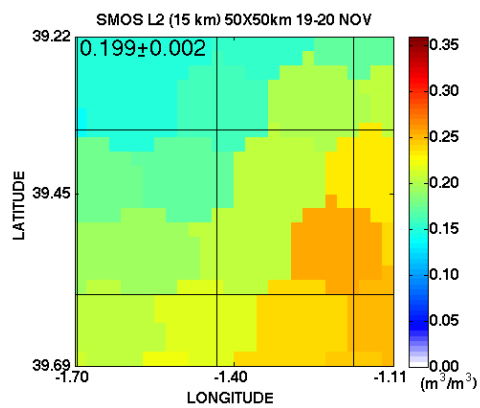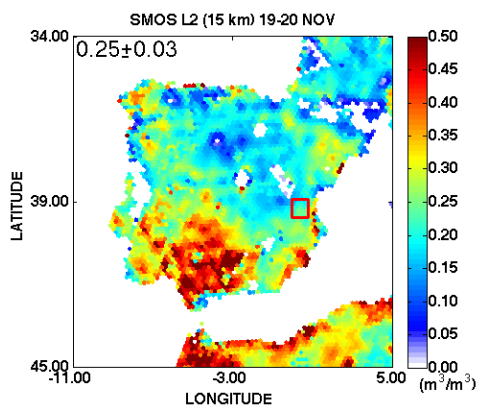
1124
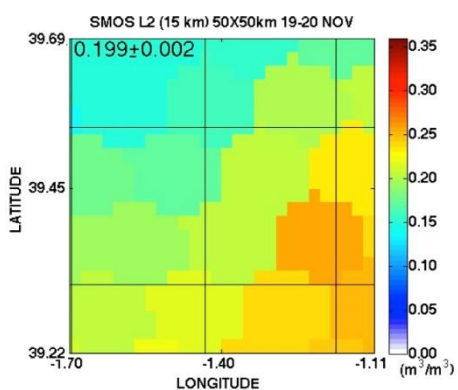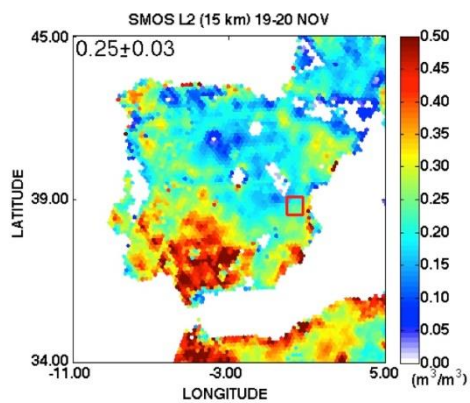
1125
1126
1127
1128
1129
1130
1131
1132
1133
1134
1135
1136
1137
1138
1139
1140
1141
1142
1143
1144
1145
1146
1147
1148
1149
1150
1151
1152
1153
1154
1155
1156
1157
1158

1159

1160   (c)
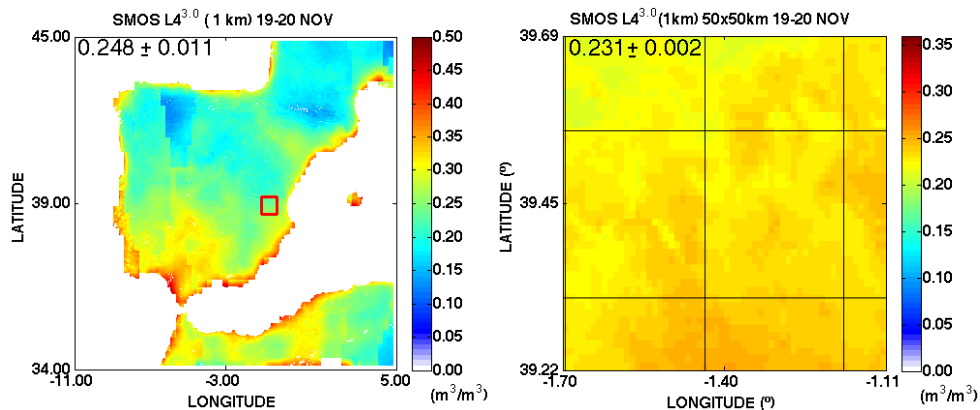
1161
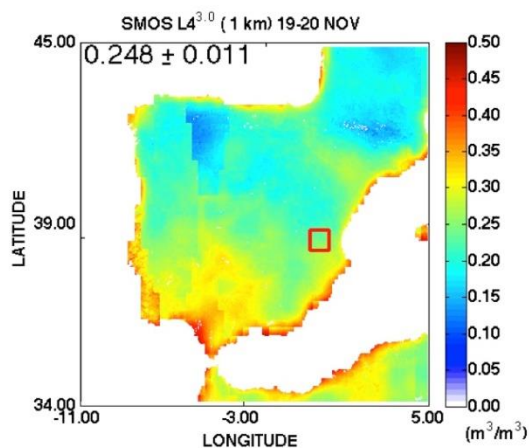
1162

1163

1164   **Figure 4:** Spatial distribution of SMOS-derived soil moisture (merged product: ascending and
1165   descending orbits are considered) over the Iberian Peninsula (left) and the VAS (right) as a
1166   mean for the 19-20 November of 2012 (a) SMOS-L3 (~25 km), (b) SMOS-L2 (~15 km), (c)
1167   SMOS-L4[3.0] (~1 km). White empty pixels in (a) and (b) are indicative of a lack of data. Please
1168   be aware of the different colour scale used for the IP and VAS.

1169

1170

1171

1172

1173

1174

1175

1176

1177

1178

1179   (a)
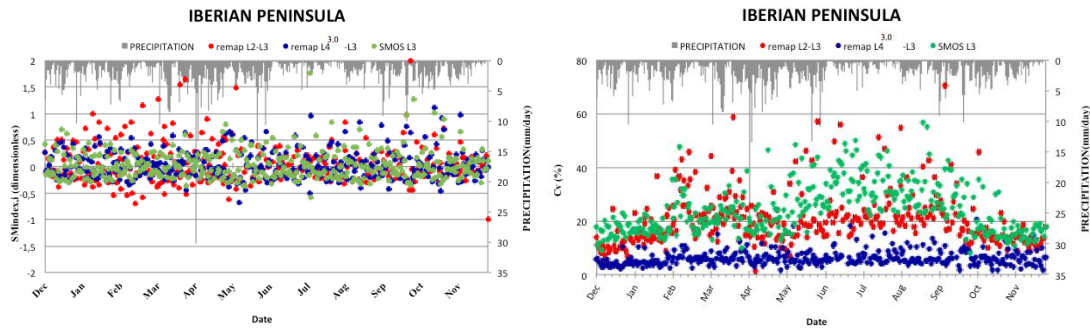
1180

1181

1182   (b)
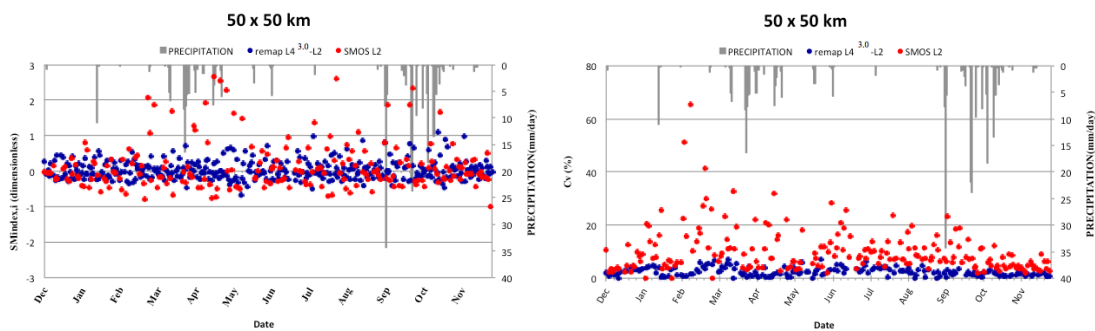
1183

1184   (c)
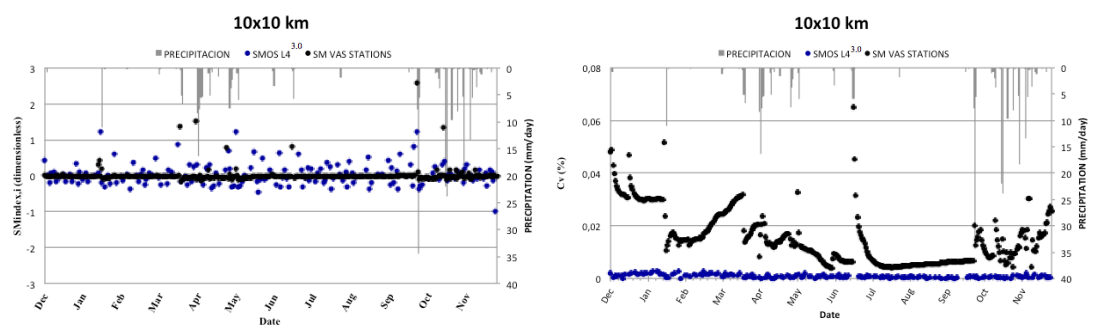
1185

1186   **Figure 5**: Averaged SMOS products and averaged ground-based observations of soil
1187   moisture evolution over the Iberian Peninsula (IP; top), the VAS area (centre), and the OBS
1188   area (bottom). Descending orbits are used. Precipitation from AEMET rain gauges on top.
1189   Left) Soil moisture daily index ($\Theta_{v\ index,i}$; dimensionless) and right) Coefficient of variation (Cv,
1190   %).

1191

1192

1193

1194

1195   (a)

IBERIAN PENINSULA
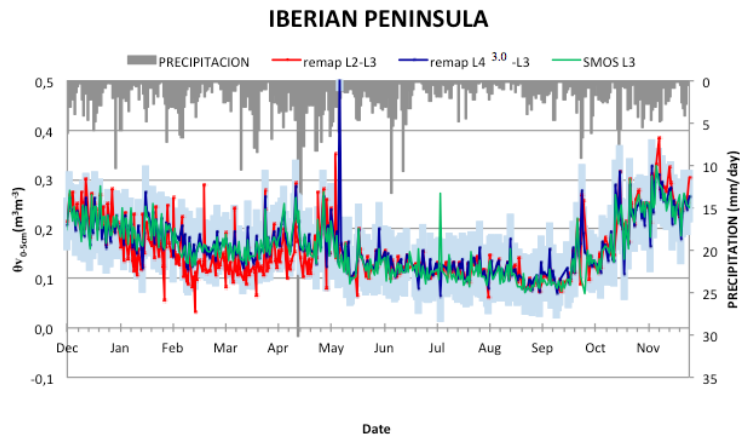
1196

1197   (b)
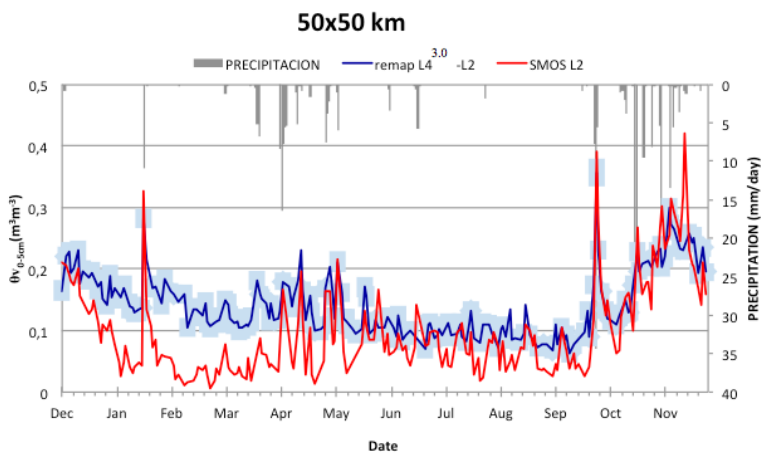
50x50 km

1198

1199   (c)
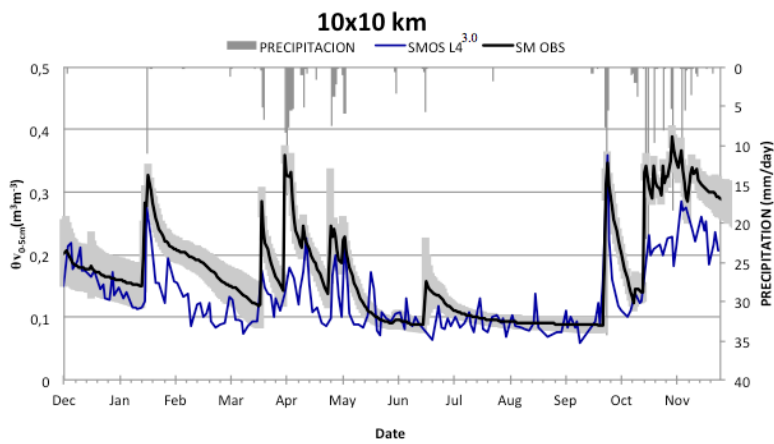
10x10 km

1200

1201   **Figure 6:** Temporal evolution of surface soil moisture time series averaged over the Iberian
1202   Peninsula (top), the VAS area (50 x 50 km^2; centre) and the OBS area (10 x 10 km^2; bottom).
1203   SMOS afternoon orbits are considered. Daily mean precipitation from the AEMET stations is
1204   shown on top of each plot. SMOS and remapped SMOS products are indicated in the plots.
1205   Shaded areas show standard deviations, respectively.

1206

1207

1208

1209

1210

1211

1212

1213

1214

1215

1216

1217

1218

1219

1220

1221

1222

1223

1224

1225

1226

1227

1228

1229

1230

1231

1232   (a)
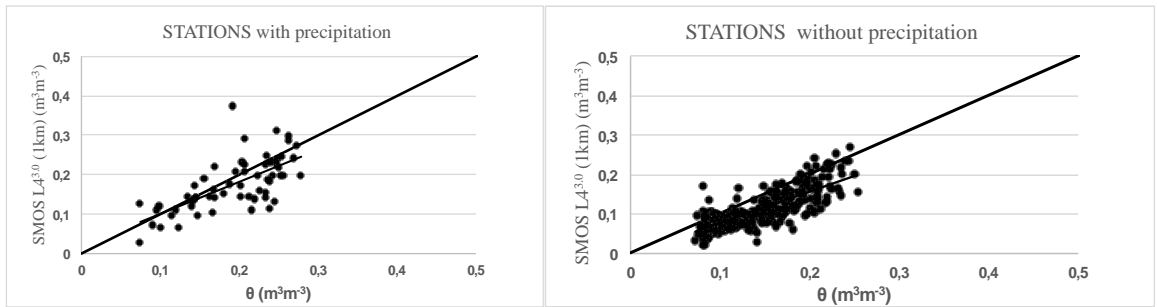
1233

1234

1235   (b)
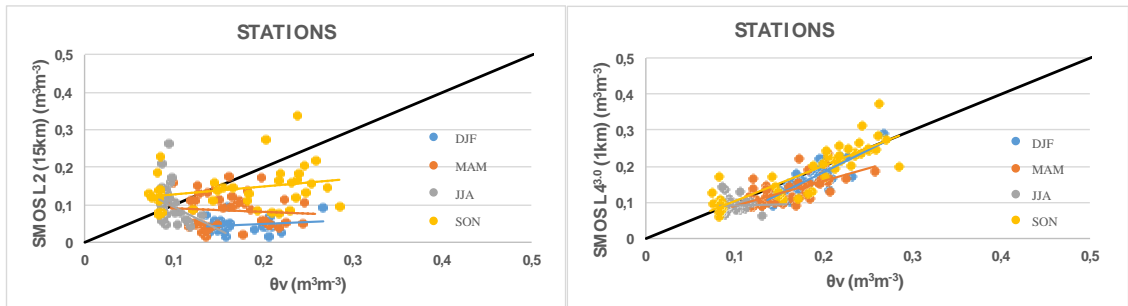
1236

1237

1238   (c)

1239
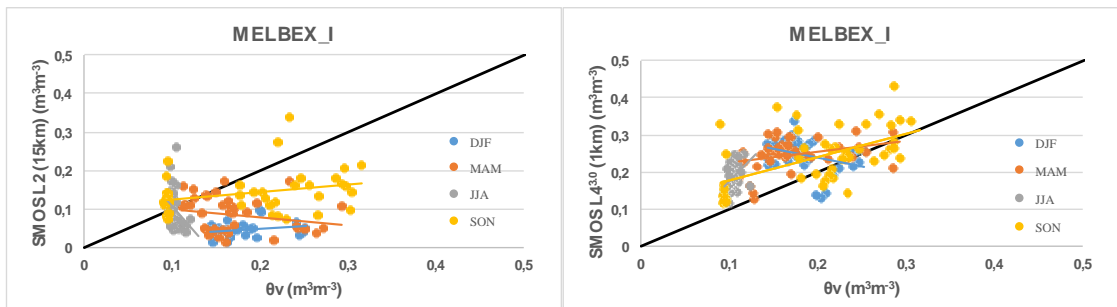
1240

1241

1242   **Figure 7:** Results of the seasonal analysis for the hydrological year starting in December
1243   2011. Scatter plots of (a) SMOS-L4[3.0] SSM (ascending and descending orbits) versus
1244   averaged 10x10 km^2 in situ soil moisture measurements (left) for days with precipitation, and
1245   (right) and without precipitation (< 1 mm /d). (b) SMOS-L2 and SMOS-L4[3.0] SSM (descending
1246   orbits) versus averaged 10x10 km^2 in situ soil moisture measurements. (c) SMOS-L2 and
1247   SMOS-L4[3.0] SSM (descending orbits) versus point-like ground measurements from

1248 MELBEX_I station, using the closest grid point. Segments are linear fit of seasonal data (3

1249 months data). Statistics for individual comparisons at all stations are summarized in Table 3.

1250

1251 (a)
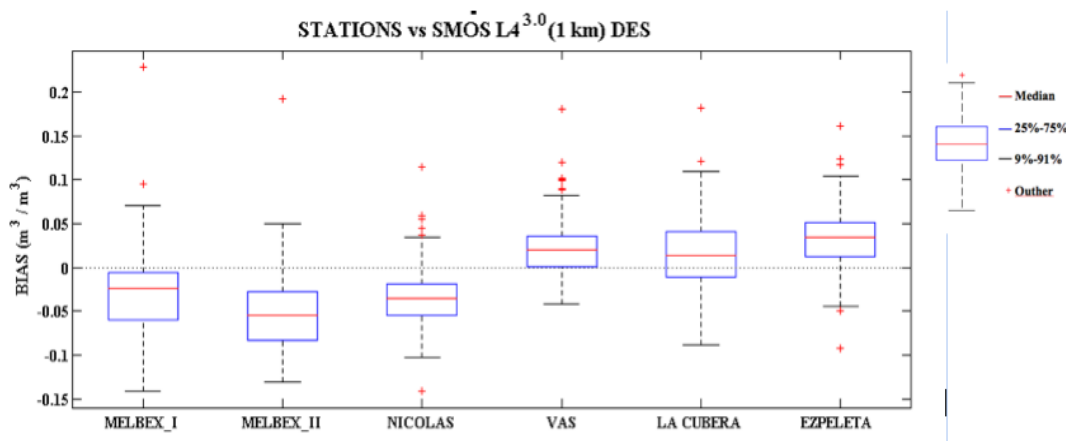
1252

1253

1254 (b)
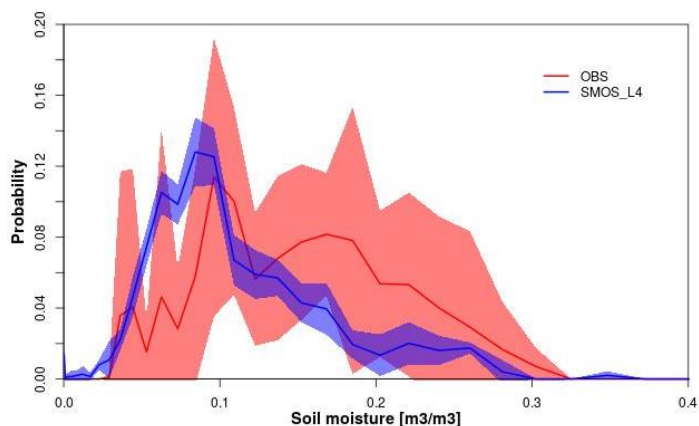
1255

1256 **Figure 8:** (a) Box plot of the comparison between point-like ground measurements at all
1257 stations over the VAS area and closest SMOS-L4$^{3.0}$ SSM data. (b) Probability distribution
1258 funtion (PDF) of SSM from in situ observations and SMOS- L4$^{3.0}$ SSM measurements. The
1259 standard deviations are indicated with shaded areas. Full lines represent the mean over all
1260 ground stations and over the 10 x 10 km^2 of the OBS area in VAS where the in SSM network
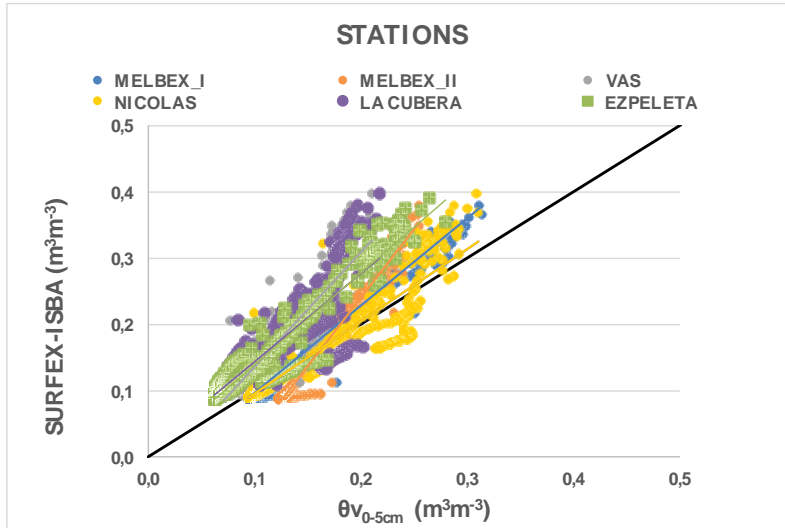1261 is located.

1262

1263

1264

1265

1269

1270

1271 **Figure 9**: Scatter plot of temporal mean (over the whole simulation period) SSM ground
1272 measurements versus SURFEX(ISBA) simulations (realistic initial scenario; REAL-I) at all
1273 stations. Statistics for all stations using the REAL-I initial scenario are presented in Table 4.

1274

1275
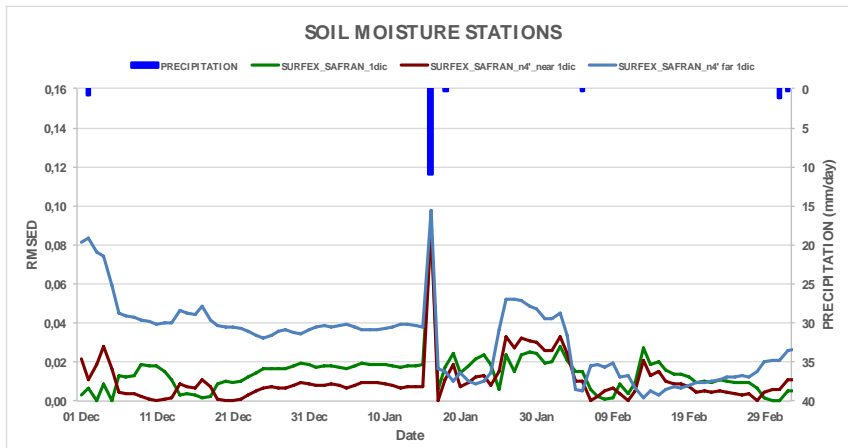
1276

1277

1278

1279

1280

1281

1282
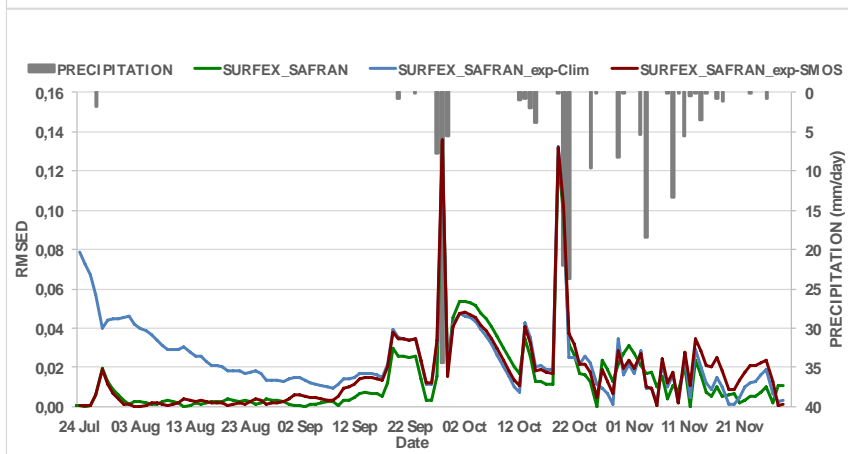
1283

1284

1285

1286
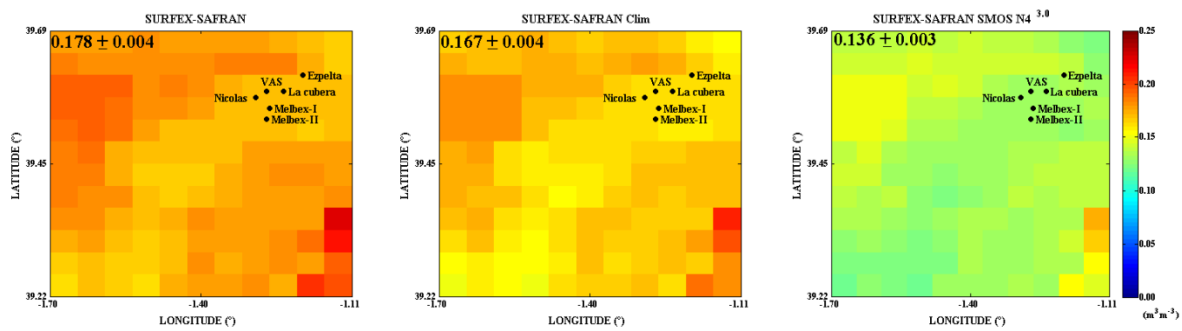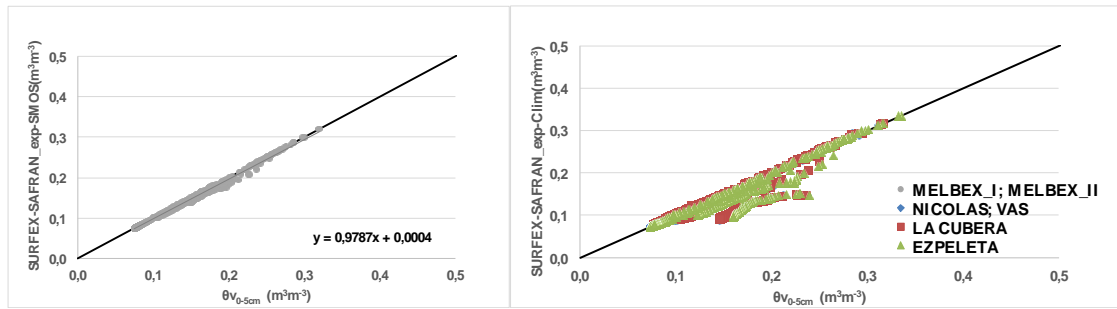
1287

1288

1289

1290

1291 (a)

1292

1293

1294

1295 (b)

1296

1297

1298

1299

1300

1301

1302

1303　(c)

1304

1305

1306

1307

1308　**Figure 10:** (a) RMSD for the daily mean SSM from the three $\mathrm{SURFEX(ISBA)}$ simulations
1309　with perturbed initial SSM scenarious (details in section 4.3.2). (b) Spatial distribution of
1310　mean SSM for the winter simulation (a, left) for the 3 simulations. (c) Scatter plot depicting
1311　the compariosn between in situ SSM observations and SURFEX-SAFRAN-SMOSL4[3.0]
1312　simulations, as a mean over all stations (left) and for each of the stations (right).

1313

1314

1315

1316